Orthogonal Polarization Fiber Optic Gyroscope with Improved Bias Drift

by

Melody A. Lynch

Submitted to the Department of Electrical Engineering and Computer Science

in Partial Fulfillment of the Requirements for the Degree of

Master of Engineering in Electrical Engineering and Computer Science

at the Massachusetts Institute of Technology

May, 1999

[June 1999]

© 1999 Melody A. Lynch. All rights reserved.

The author hereby grants to M.I.T. permission to reproduce and
distribute publicly paper and electronic copies of this thesis
and to grant others the right to do so.

Author ....
Department of Electrical Engineering and Computer Science

Certified by ....
H. A. Haus
Institute Professor
Thesis Supervisor

Certified by ....
W. Kelleher
The Charles Stark Draper Laboratory, Inc.
Technical Supervisor

Accepted by ....
Arthur C. Smith
Chairman, Department Committee on Graduate Theses
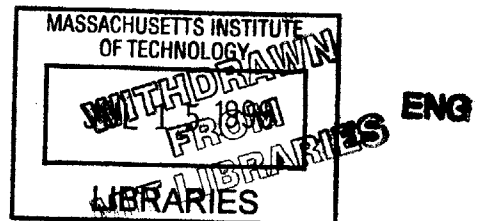
1

Orthogonal Polarization Fiber Optic Gyroscope with Improved Bias Drift

by

Melody A. Lynch

Submitted to the
Department of Electrical Engineering and Computer Science

May, 1999
In Partial Fulfillment of the Requirements for the Degree of
Master of Engineering in Electrical Engineering and Computer Science

Abstract

The orthogonal polarization gyroscope (OPFOG) is a novel gyroscope that does not require a phase bias in the fiber ring. By exploiting two orthogonal polarization states such that they propagate along a single axis in a polarization maintaining (PM) optical fiber coil a sensitive gyroscope can be developed. However, thermally induced birefringence changes in the biasing element degrades the bias drift performance of the instrument. This thesis explores a method to actively measure the thermal error and remove it numerically. The temperature monitored OPFOG was constructed and characterized for bias drift and angle random walk performance. The temperature monitored OPFOG shows improved bias drift over the original instrument.

Acknowledgment

May, 1999

5/13/99

Melody A. Lynch   Date

TABLE OF CONTENTS

TABLE OF FIGURES

Chapter 1   Introduction

1.1   Motivation

The first gyroscopes were mechanical spinning mass gyroscopes. Other mechanical gyroscopes include the tuning fork gyroscope and resonator gyroscopes. However, these systems involve moving parts, which shorten the lifetime of the instrument. By moving to a fiber optic gyroscope (FOG), many advantages can be reaped: longer reliability and lifetime, ability to withstand shocks and vibrations, large dynamic range, and very fast startup times. By utilizing large fiber coils, extremely accurate rates can be measured. Hence, the FOG can be used for tactical grade applications, as well as aeroplane and ship navigation.

The FOG does not have the size advantages of mechanical gyroscopes. The technology of micro-machining electronics can be directly transferred to mechanical gyroscopes, while the fiber coil of the FOG imposes a limit upon the minimum size of the instrument. However, new technology in micro-machining optical components makes it possible to reduce the size of current FOGs if the majority of the components are bulk optical devices.

1.2   Sagnac Effect

The fiber gyroscope is based upon the Sagnac effect, which is defined as a phase shift in counter-propagating light waves around a rotating closed path. For a system at rest, the two light waves return in phase traveling at a constant velocity, c. Under rotation, the counter-rotating path is shorter than the co-rotating one, as shown in Figure 1. Therefore, one wave will take a shorter amount of time to arrive at the starting point. By interfering the two waves, a phase time difference, $\Delta\phi$, is measured which is proportional to the rotation rate, Ω. The Sagnac phase difference becomes

$$\Delta\phi = \frac{2\pi L D}{\lambda c} \cdot \Omega \qquad (1)$$

where λ is the wavelength of light in a vacuum, D is the coil diameter, and L is the fiber length. Since the waves are traveling at the speed of light, the Sagnac effect is very small. An enhancement of the effect is obtained by enlarging the area around which the waves travel.
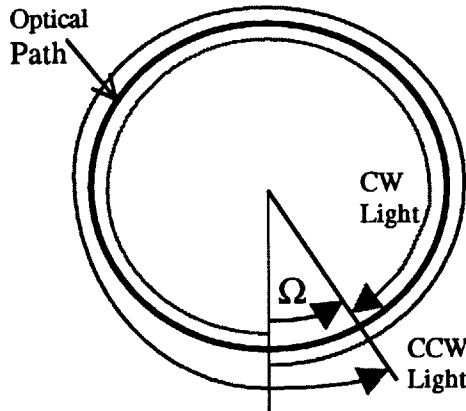
Figure 1: Sagnac effect with rotation rate Ω

Assuming a lossless 3dB beamsplitter coupling light into the fiber coil, the clockwise and counter-clockwise beams would interfere to give an output intensity that is a raised cosine function. Therefore, a phase bias of $\pi/2$ is required to operate at the point of maximum slope, which is also the maximum sensitivity point.

1.3 Interferometric Fiber Optic Gyroscope

The widely adapted interferometric fiber optic gyroscope (IFOG) architecture, shown in Figure 2, consists of a sensor coil with a phase bias modulator to maximize sensitivity and allow for optical closed loop operation. Placing the phase modulator asymmetrically within the fiber coil introduces a carrier into the signal via a non-reciprocal effect. By adjusting the carrier amplitude a maximum sensitivity bias point is established. An integrated optical circuit (IOC) phase modulator is typically the biasing mechanism of a gyroscope. The phase modulation provided by the IOC often results in a costly system with high frequency electronics to demodulate the output signal. The IOC performance requirements limit the size of the gyroscope to four inches in diameter for high

7

performance instruments. The length of the IOC also has a direct impact upon the performance of the gyroscope, hence the size limitations of the system. Angle random walk (ARW) performance of 10^{-5} deg/rt-hr and 1σ bias drift of 10^{-4} deg/hr have been achieved with the conventional IFOG.
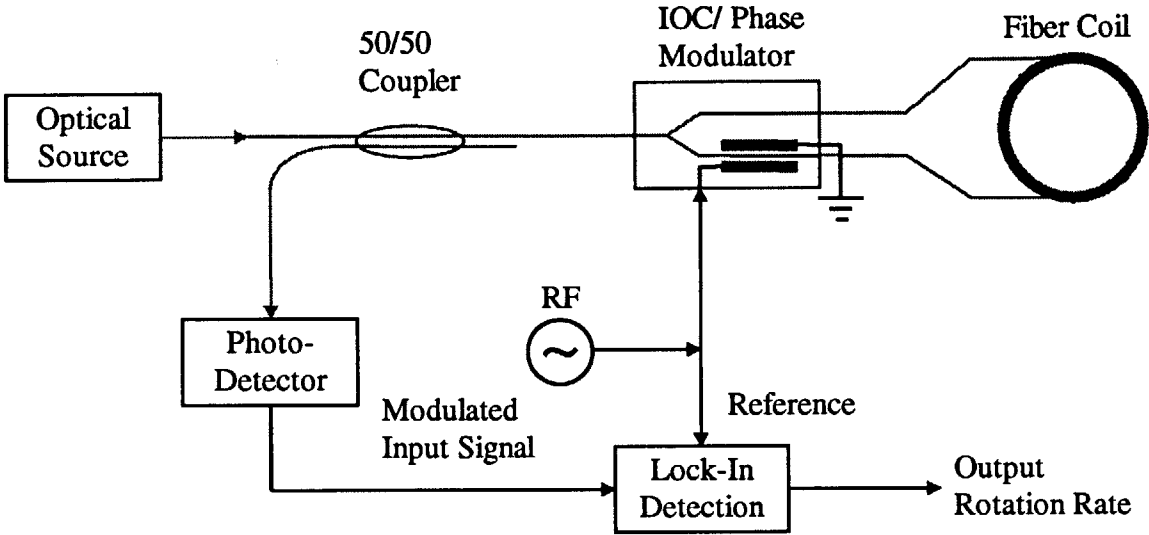
Figure 2: Conventional IFOG Configuration

Chapter 2 Orthogonal Polarization Fiber Optic Gyroscope

In 1984, Kajioka [1,2] presented a novel IFOG design, shown in Figure 3, which eliminates the modulation problems associated with the conventional IFOG. The major advantage of the orthogonal polarization gyroscope (OPFOG) is that it does not require a phase bias in the fiber ring. By eliminating the IOC, the size of the gyroscope can be reduced to a diameter of 2". The OPFOG uses to its advantage two orthogonal polarization states such that they propagate along a single axis in a polarization maintaining (PM) optical fiber coil.
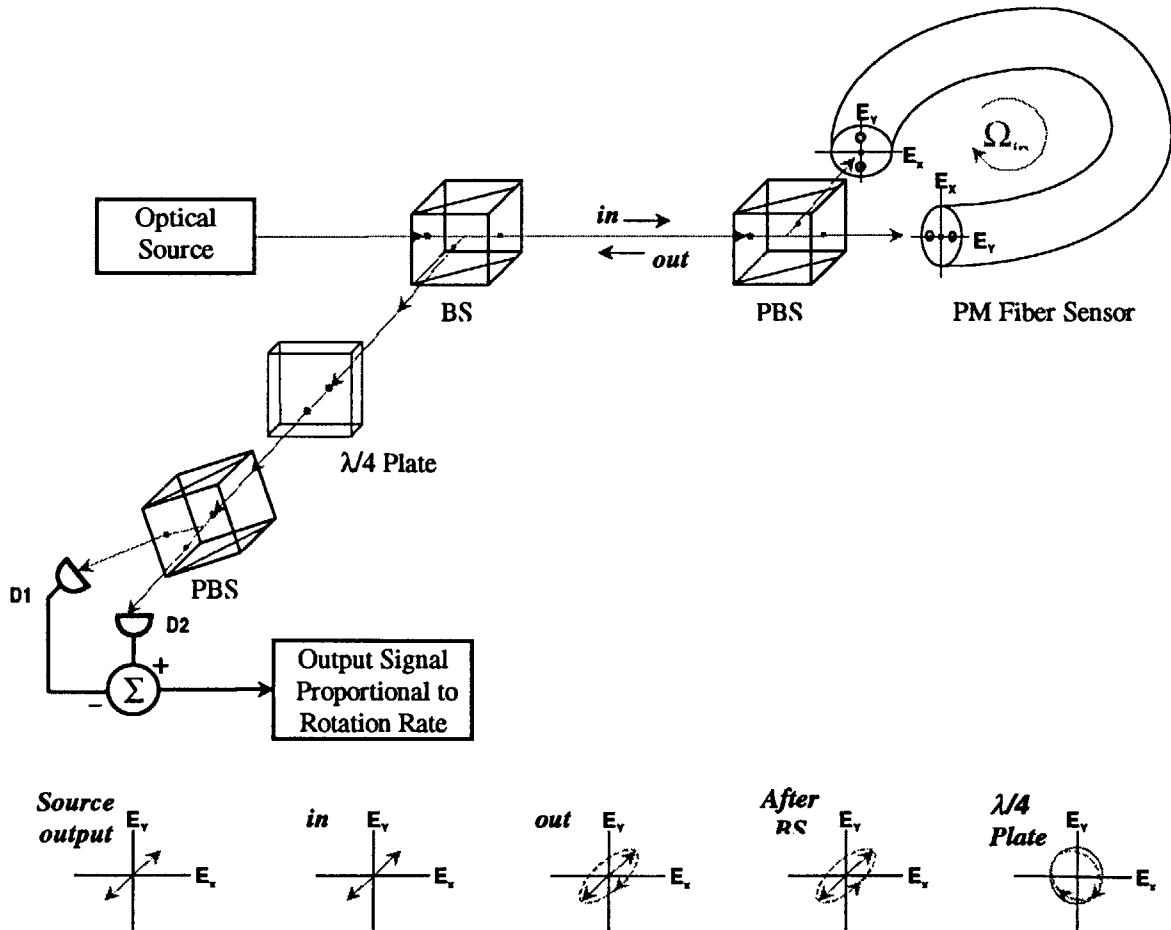
Figure 3: Conceptual Schematic of Kajioka's Original OPFOG. The insets display the polarization states at various locations along the optical train. The solid line represents the system under no rotation, while the dashed line represents ring rotation.

2.1 Principle of OPFOG Operation

The concept of the original OPFOG is shown above. This architecture is the basis for all further improvements. The input light, linearly polarized at 45°, is split from the source via a non-polarizing beamsplitter (BS), which later acts as an output coupler, into a polarizing beamsplitter (PBS). The PBS splits the input beam into two orthogonal waves, which propagate in opposite directions around a PM sensor coil. The two orthogonal modes travel along the same birefringence axis. This is accomplished by orienting the slow axis, E_Y, of the fiber coil parallel to the PBS output polarization mode. After traversing the fiber coil, the two modes are recombined at the PBS, but are not mixed at this point, as in the conventional IFOG. A portion of the returning light is reflected by the BS to a balanced detector.

Under no rotation, the output of the sensor coil is still linearly polarized. However, when the coil is rotated the output becomes elliptically polarized due to the added Sagnac phase, which can be seen in the insets of Figure 3. The Sagnac phase information is contained in one polarization, while the orthogonal mode is a reference. One polarization mode can be thought of as a local oscillator, while the orthogonal polarization represents the signal. The rotation signal can be biased outside of the ring by a quarter-wave plate because both modes are still accessible outside of the sensor coil. The waveplate is oriented such that there is a $\pi/2$ relative phase shift between the modes. The two waves are mixed at a detector beamsplitter at 45° and then undergo balanced detection. The difference in the measured power is proportional to the gyroscope rotation rate at its most sensitive operating point.

2.2 Improvements upon the OPFOG

The original OPFOG has an advantage over the conventional IFOG in that it does not require a phase bias in the ring and it effectively cancels intensity noise by balanced detection. However, if the retardation of the biasing waveplate changes due to source

wavelength shifts or temperature induced birefringence changes first order errors will occur in the rotation signal.

In 1994, Doerr [3,4] improved upon the above OPFOG by removing these false rotations to first order. These false rotation signals were due mainly to temperature variations in the environment. Temperature variations across elements induce a local birefringence change in the material. The stability of the OPFOG is dependent upon two critical components, the output port of the NPBS and the detector PBS. These elements are especially sensitive because the light only traverses them in one direction. Elements that are traversed twice are not as critical because each mode travels through the material in both birefringence axes. Take for example the PM spatial filter shown in Figure 4, one mode will traverse the fast axis while being launched into the fiber coil, then traverse the slow axis after transmission through the coil. The temperature variations are much slower than the propagation time though the system. The local birefringence variations induce a phase difference between the orthogonal modes, which appears as a false rotation at the gyroscope output. By replacing these elements with environmentally stable ones, Doerr was able to design a system that eliminated first order false rotation rates.

In this system, shown in Figure 4, the input NPBS from Figure 3 is replaced by a prism at Brewster's angle. The optical train is designed to have no material between the output splitting point and the quarter-waveplate bias, which is accomplished by a special prism. By eliminating the material beyond the output splitting point, local birefringence variations can be avoided after the beam has acquired the Sagnac phase shift. The silica prism acts like a special beamsplitter, transmitting all of the TM polarization, and both reflecting and transmitting the TE polarization at less than 50%. By launching vertically (TE) polarized light into the system, the gyroscope operates in a manner similar to the original OPFOG. However, there is a slight reduction in the local oscillator signal because losses are incurred through the reflection port of the prism.
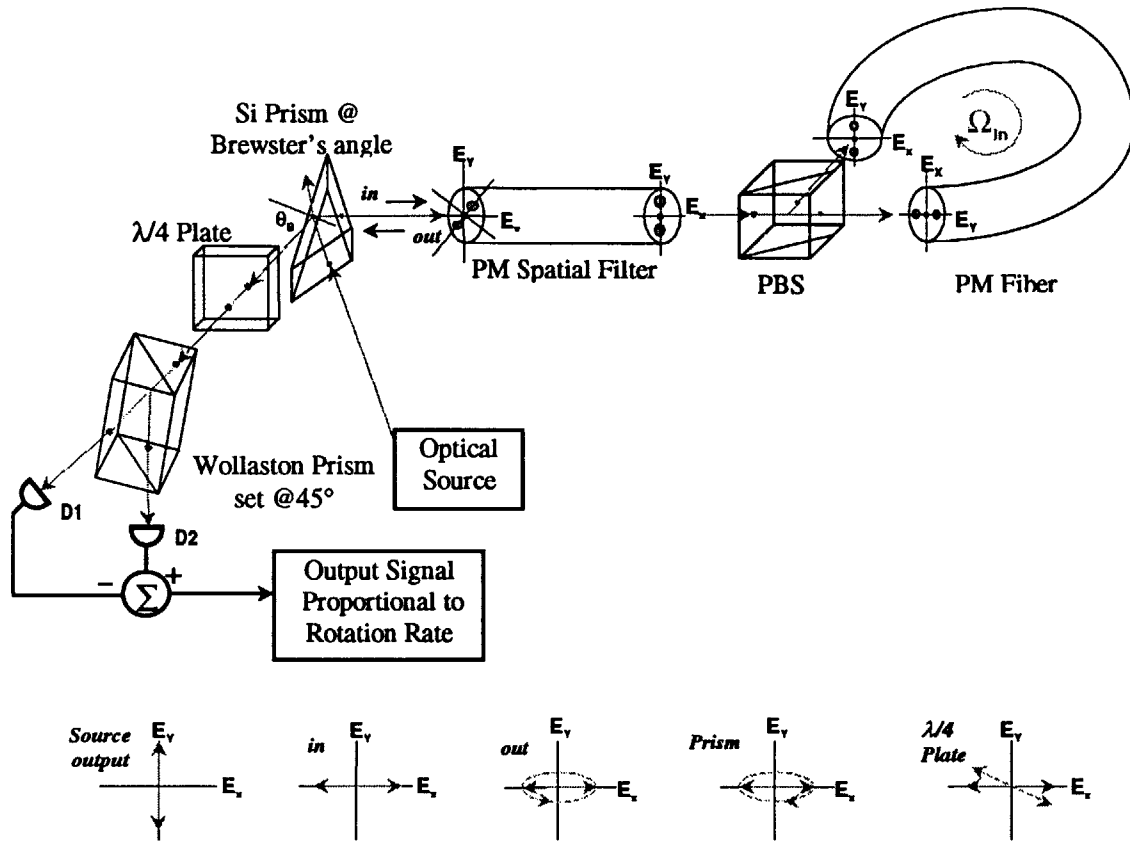
Figure 4: Conceptual Schematic of Doerr's
OPFOG Configuration

Another modification made by Doerr is to replace the detector PBS with a
birefringent wedge, the Wollaston prism as shown in the above figure. This wedge
eliminates excess phase delay due to local birefringence changes in the beamsplitter
because both polarization modes travel the same distance within the same material in the
prism. In a normal PBS, the two modes are split and travel in different glass wedges,
which will introduce a false rotation rate when there is a temperature variation. The
Wollaston prism has the same functionality as the PBS, but the two output modes are only
separated spatially by 15°, instead of by 90°, and temperature sensitivity is not introduced.

By using this architecture, first order false rotation rates have been eliminated.
However, a change in source wavelength or a temperature change will still cause an error
in the phase bias of the quarter-wave plate. This, in turn, affects the performance of the

gyroscope. By monitoring the phase bias of the quarter waveplate as it varies with the environment, the false rotation rates associated with it can be eliminated numerically.

2.3   Temperature Monitored λ/4 Waveplate OPFOG

One error source, mentioned above, is temperature-induced fluctuations affecting the waveplate bias retardation. By performing a Jones matrix analysis on the Doerr OPFOG, the dependence of the output rotation signal upon the biasing error was found to be

$$P_{out} = \cos(\varepsilon_{qwp}) \; \sin(2\phi) \qquad\qquad (2)$$

where P_{out} is the output of the balanced detector circuit, ε_{qwp} is the retardation error of the quarter waveplate, and ϕ is the actual rotation rate.

For example, consider a 5 °C temperature change (lab environment) of a zero-order λ/4 plate made of quartz. Such a plate was used to provide maximum sensitivity bias in the OPFOG experiment. According to the manufacturer, the retardation error due to temperature is 0.0001 λ/°C. This retardation error of 3.1E-3 rad corresponds to an output error of 4.9 ppm in the instrument scale factor.

The retardation waveplate is also wavelength dependent. If the optical source wavelength changes then the phase bias provided by the waveplate introduces a higher-order scale factor error. For example, if wavelength changes 1 ppm in the optical source, this will result in less then 1 ppm scale factor change.

One way to reduce this error further is to monitor the phase bias retardation of the quarter waveplate and actively remove the error associated with it. Only elements that are not traversed by both polarization modes need to be included. Furthermore, both the signal and monitor paths should be as similar as possible. Ideally these paths should use the same components. The proposed system is shown in Figure 5. In this configuration, part of the source light has been diverted to monitor the quarter waveplate retardation. As mentioned above, the sensing path is neglected and the same components are used for both the signal and monitor paths.
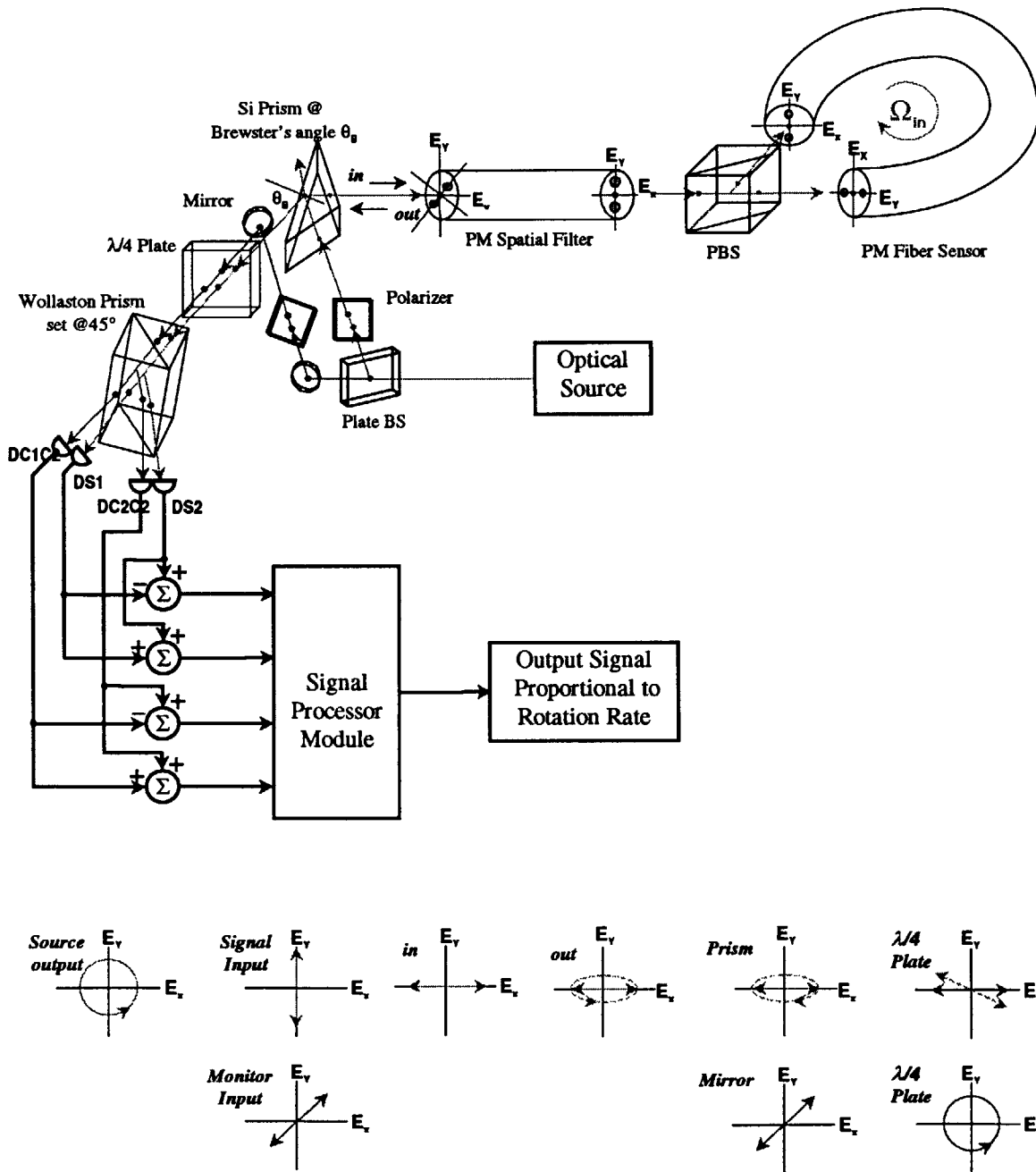
Figure 5: OPFOG with Temperature Error Monitoring.

3.1   Quarter Waveplate Phase Drift Measurement

A benchtop experiment was devised to determine whether the retardation error due to temperature could be reliably measured. A system similar to the proposed OPFOG monitor was constructed as illustrated in Figure 6. A small thermal oven enclosed a zero-order quartz quarter waveplate so that temperature could be accurately controlled and recorded. The temperature controller is capable of controlling the oven to within $0.2°$ C. A thermistor was placed upon the waveplate to monitor its temperature fluctuations. The other components, which do not affect the experiment, were exposed to the room temperature of the lab, which varies approximately $5°$ C. These components were not temperature controlled. An opaque box enclosed the entire testbed to eliminate noise from the ambient light of the lab.
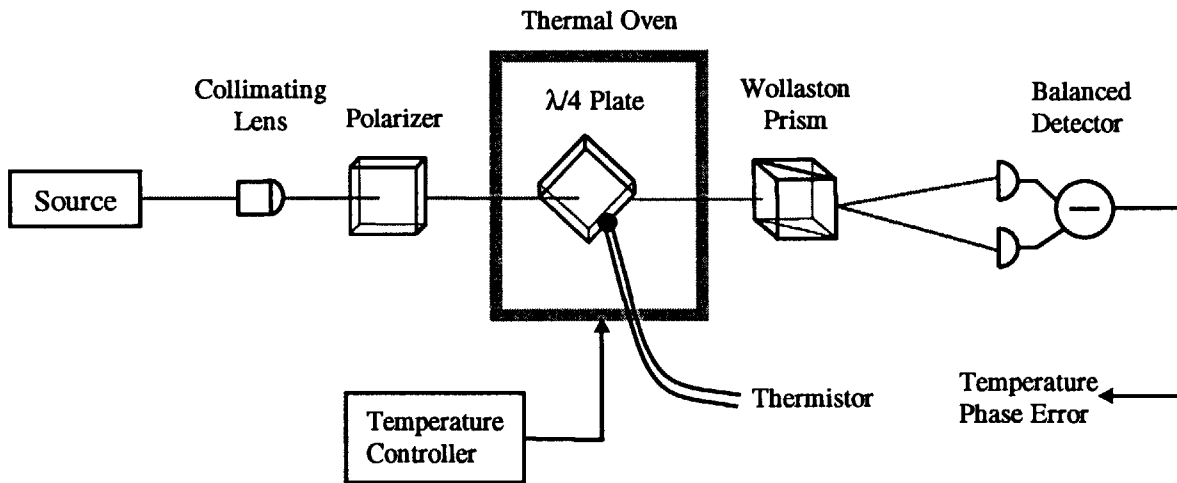
Figure 6: Quarter Waveplate Phase Drift with Temperature Experiment

In the experiment, a polarizer is used to linearly polarize the source output. The linearly polarized light is launched into the quarter waveplate such that the output is circularly polarized. The Wollaston prism separates the two orthogonal polarizations, which are detected by the detectors.

15

The expected output of the experimental setup was derived using Jones Matrixes. The Jones Matrix representation of a quarter waveplate is

$$
J_{qwp} = \begin{pmatrix} \cos(-\theta) & \sin(-\theta) \\ -\sin(-\theta) & \cos(-\theta) \end{pmatrix} \cdot \begin{pmatrix} e^{j(\frac{\pi}{2}+\varepsilon)} & 0 \\ 0 & 1 \end{pmatrix} \cdot \begin{pmatrix} \cos\theta & \sin\theta \\ -\sin\theta & \cos\theta \end{pmatrix} \tag{3}
$$

where θ is the quarter waveplate rotation angle, and ε is the retardation error due to temperature. For this experiment, the angle θ was set at 45°. Ideally the output will be circularly polarized if there is no retardation error. Since the light is perfectly circular, the amplitudes of the two polarization modes are the same. Therefore, the output of the detector should be completely balanced by subtracting the two detectors, $D1$ and $D2$, which monitor the polarization states.

If there is a perturbation ε in the retardation of the waveplate, then the output polarization, J_{out}, will be elliptical.

$$
J_{out} = \frac{1}{2} \cdot \begin{pmatrix} 1+j\, e^{j\varepsilon} \\ -1+j\, e^{j\varepsilon} \end{pmatrix} \tag{4}
$$

The change in the output of the detector will be proportional to the retardation error in the waveplate. The intensity measured by the first detector is

$$
D1 = \frac{1}{4}\left(1+j\, e^{j\varepsilon}\right)^{*}\left(1+j\, e^{j\varepsilon}\right) \tag{5}
$$

while the intensity of the orthogonal polarization is given by

$$
D2 = \frac{1}{4}\left(-1+j\, e^{j\varepsilon}\right)^{*}\left(-1+j\, e^{j\varepsilon}\right). \tag{6}
$$

Subtracting the two signals given by Equations 5 and 6 results in a differential power, ΔP,

$$
\Delta P = D1 - D2 \tag{7}
$$

which is directly related to the retardation error due to temperature

$$
\Delta P = -\sin(\varepsilon) \tag{8}
$$

16

By using the small angle approximation for a sine curve, the output of the detector is proportional to the retardation error of the waveplate.

The output phase error of the quarter waveplate and the resistance of the thermistor were monitored to correlate phase retardation and temperature. Data was collected at seven different temperatures, six of which are shown in Figure 7. The power incident upon the two detectors was measured, taking the ratio of the sum and difference to obtain the detector output. This eliminates any errors that may occur due to source intensity fluctuations, as will be discussed later in Section 3.3. The detector output is proportional to the phase error in radians. Using the experiment outlined above, the data obtained of retardation error due to temperature is plotted in Figure 7.

The data was used to calculate a temperature sensitivity coefficient by taking the ratio of the mean phase error and mean temperature over an hour. This was performed taking every combination of pairs of temperatures, T_i and T_j, resulting in 21 calculated coefficients, α.

$$\alpha = \frac{V_i - V_j}{T_i - T_j} \tag{9}$$

where V_i and V_j are the mean balanced detector retardation error over an hour for temperatures T_i and T_j, respectively.

Using the raw data relating temperature to quarter waveplate retardation error, a temperature sensitivity coefficient was extrapolated. The calculated temperature coefficients are plotted in Figure 8 for different temperature steps. The trend in the groupings of the calculated temperature coefficients comes from a slightly non-linear retardation error from the waveplate. As the waveplate temperature increases, there is a slightly smaller relative retardation error than at lower temperatures. This causes the groupings shown in Figure 8 when the pairs of mean data points are taken. Temperature pairs that are father apart will yield a slightly lower coefficient than temperature pairs that differ by only a few degrees. It can be seen from Figure 8 that the mean measured temperature coefficient is 6.47E-4 rad/°C. This value is very close to the manufacturer-estimated coefficient of 6.28E-4 rad/°C [5].

17

This experiment is a proof that the retardation error of the quarter waveplate can be actively measured. By inserting this module into the OPFOG, the rotation rate error due to temperature fluctuation of the OPFOG biasing element can be monitored and eliminated numerically.
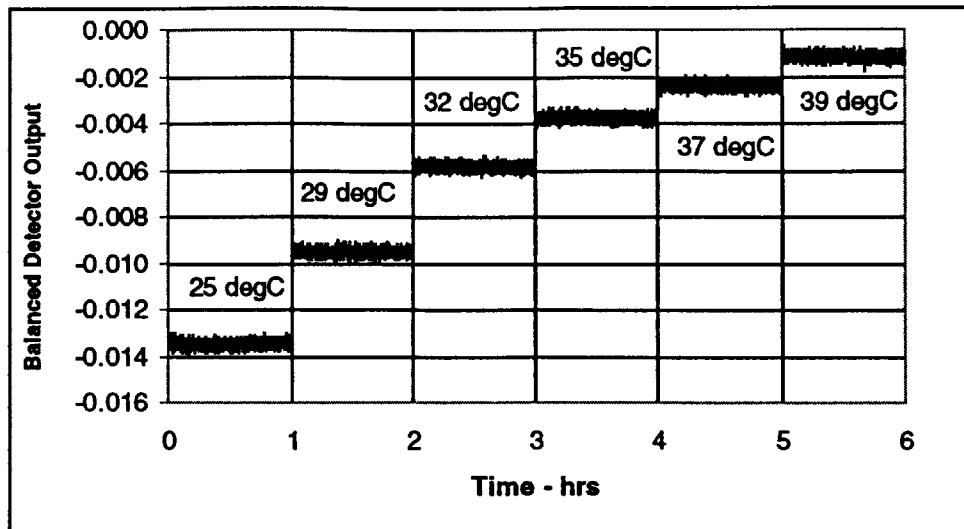
Figure 7: Waveplate Retardation Error vs. Temperature.
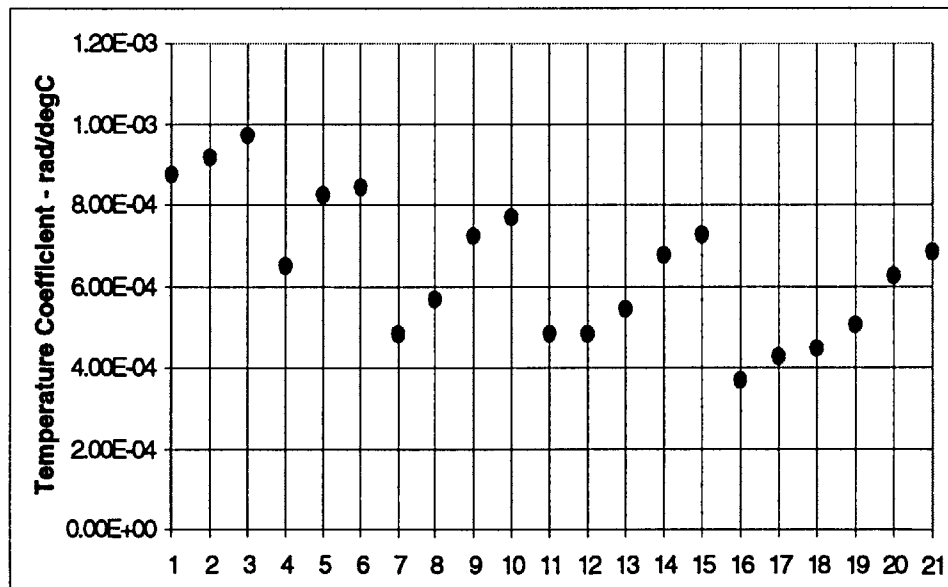
Figure 8: Calculated Temperature Coefficients for Waveplate

19
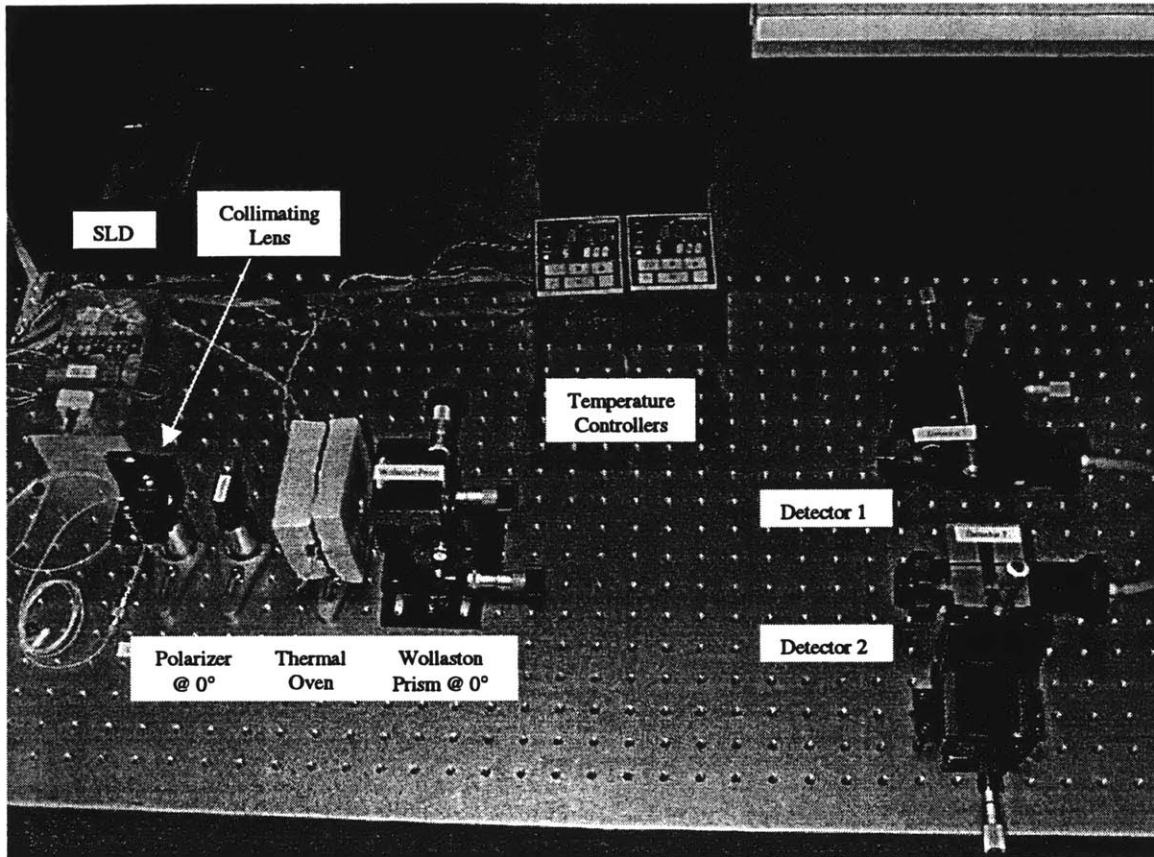
Figure 9: Photograph of Quarter Waveplate
Phase Drift Experiment; Waveplate at 45° inside
Thermal Oven

3.2   PBS Splitting Ratio Measurement

The splitting ratio of the beamplitter is important because it causes a bias error due to the Kerr Effect. This calculation is shown in Appendix A. A benchtop experiment was devised to determine the dependence of the splitting ratio upon temperature. It is very similar to the quarter waveplate experiment discussed in Section 3.1. The same test conditions were used in the experiment as in previous experiment, except the thermal oven enclosed the beamsplitting module. A schematic of the system is depicted in Figure 10.
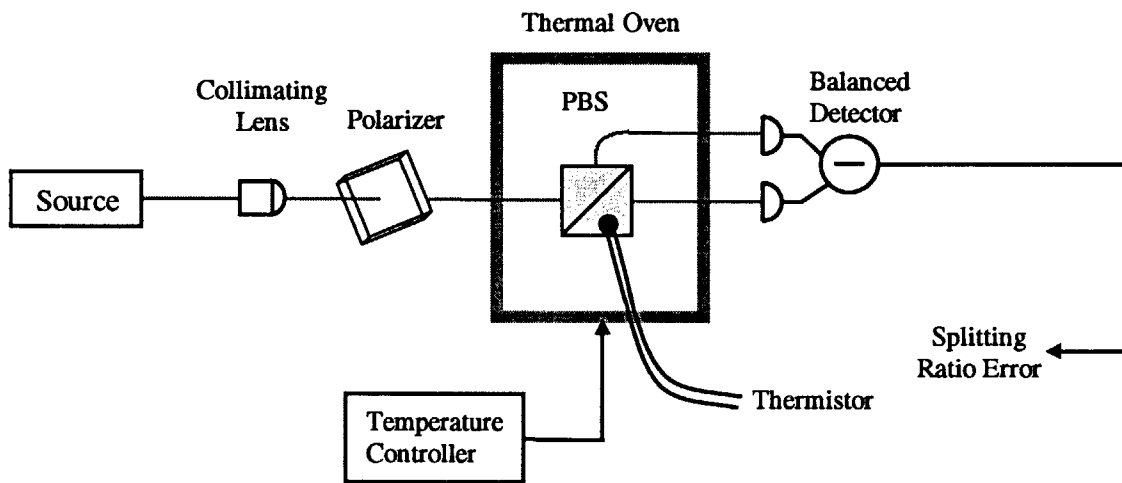
Figure 10: PBS Splitting Ratio with Temperature Experiment

In the experiment, a polarizer is used to create linearly polarized light at 45°. The linearly polarized light is launched into the polarizing beamsplitter's fiber such that there is an equal amount of light coming out of the two output ports. The two detectors measure the power from the output ports.

The splitting error of the beamsplitter and the resistance of the thermistor were monitored to correlate splitting error and temperature. The data was collected at five different temperatures. The power incident upon the two detectors was measured, taking the ratio of the sum and difference to obtain the detector output. This eliminates any errors that may occur due to source intensity fluctuations, as will be discussed in the next

section. The detector output is proportional to the percent split error. Using the experiment outlined above, the data is plotted in Figure 11.

Using the raw data relating temperature to splitting error, a temperature sensitivity coefficient was extrapolated, shown in Figure 12. Ideally the temperature dependence is zero. However, the temperature coefficient was found to be 0.082 % split/degC. Here, the percent split is the change in one arm of the splitting ratio. For example, is the device moves from a 50/50 split to a 49/51 split, the change in the percent split is 1%.

The gyroscope bias error due to the Kerr effect [6,7], Ω_{Kerr}, is dependent upon the splitting ratio, k_s, of the beamsplitter

$$\Omega_{Kerr} = \frac{2\,c\,\eta\,n\,\delta}{D\,A_{core}} \cdot (1 - 2k_s) \cdot \frac{P_o}{N_{modes}} \tag{10}$$

where $\eta n \delta$ is the Kerr coefficient of silica fiber, D is the coil diameter, A_{core} is the area of the fiber core, P_o is the power into the beamsplitter, and N_{modes} is the number of modes in the source. For this system an approximate Kerr coefficient for the fiber is 10^{-14} $\mu m^2/\mu W$, a coil diameter of 6.8", core diameter of 9μm, power of 63μW, and 10^4 modes were used. For the measured coefficient of the beamsplitter, a bias due to the Kerr effect of 1.25E-6 °/hr /Δ°C occurs.
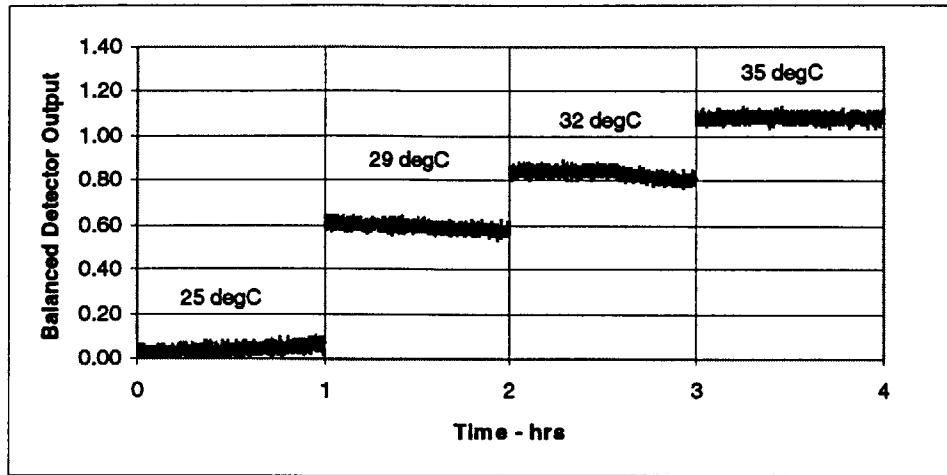
Figure 11: Beamsplitter Retardation Error vs. Temperature.
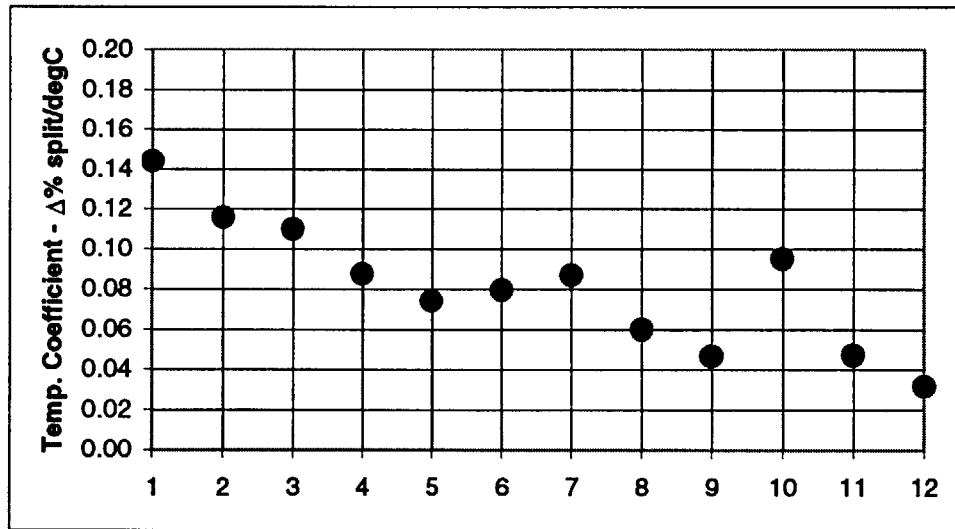
Figure 12: Calculated Temperature Coefficients for Beamsplitter
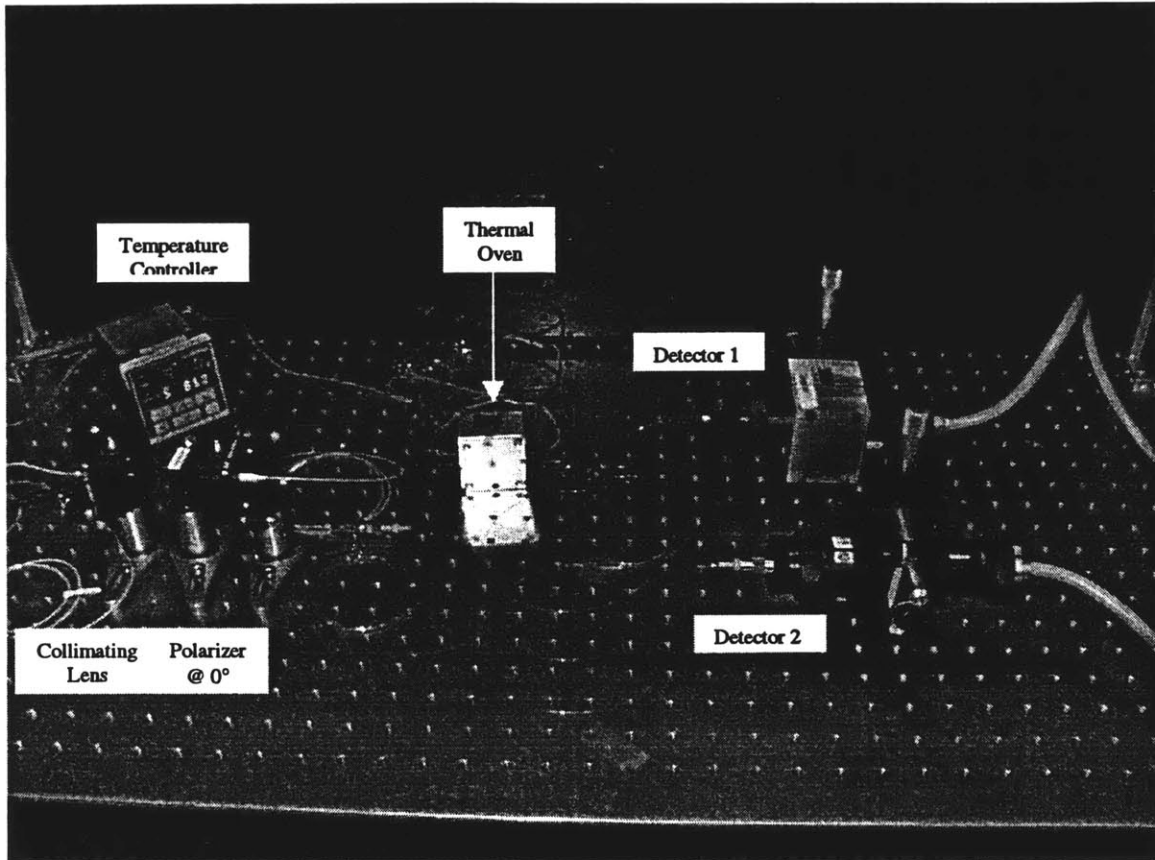
Figure 13: Photograph of Beamsplitter Splitting
Ratio with Temperature Experiment;
Beamsplitter in Thermal Oven

3.3 Source Intensity Fluctuations

If the source intensity, I_s, fluctuates, then the scale factor, K

$$K = \frac{\lambda \, c}{2 \, \pi \, L \, D} \cdot I_s \qquad (11)$$

of the gyroscope will also change. One way to eliminate this phenomenon is to measure the intensity at the output, then divide it out of your output signal. This is practically done by taking the ratio of the difference and sum of the detectors. The difference gives you the rotation rate information, while the sum gives the total intensity from the source. A drawback to this configuration is that it reintroduces the excess intensity noise that was significantly reduced by balanced detection [8]. While the system has large noise sources, the extra noise in not dominant. However, as the noise floor approaches the shot noise limit, it will become a major source of noise in the system, limiting the resolution of the gyroscope. If this is the case, a control loop will have to be added to stabilize the source intensity.

This phenomenon was discovered when doing temperature experiments upon the gyroscope. The output changed significantly during an overnight test run. It was surmised from the time at night that the output started changing that the change was occurring when the air-conditioning was turned off at night. To determine which component was heavily temperature dependent, a heat gun was aimed at each element until the gyroscope output noticeably changed. The high-powered SLD with an exposed fiber pigtail, shown in Figure 15, was the sensitive element.

A thermistor was placed upon the pigtail and the source power and temperature were measured. The data is shown in Figure 14. This data, which was taken overnight, shows a distinct correlation between room temperature and output power. As the temperature of the pigtail increases, the output power of the SLD decreased. The temperature caused a misalignment of the SLD chip output and the fiber pigtail, whose placement varies due to expansion of the epoxy holding the pigtail. Replacing the SLD with an Anritsu SLD, which does not have an exposed fiber pigtail, solved this problem. The Anritsu SLD, described in Section 4.1, has an output power that is stable with temperature.
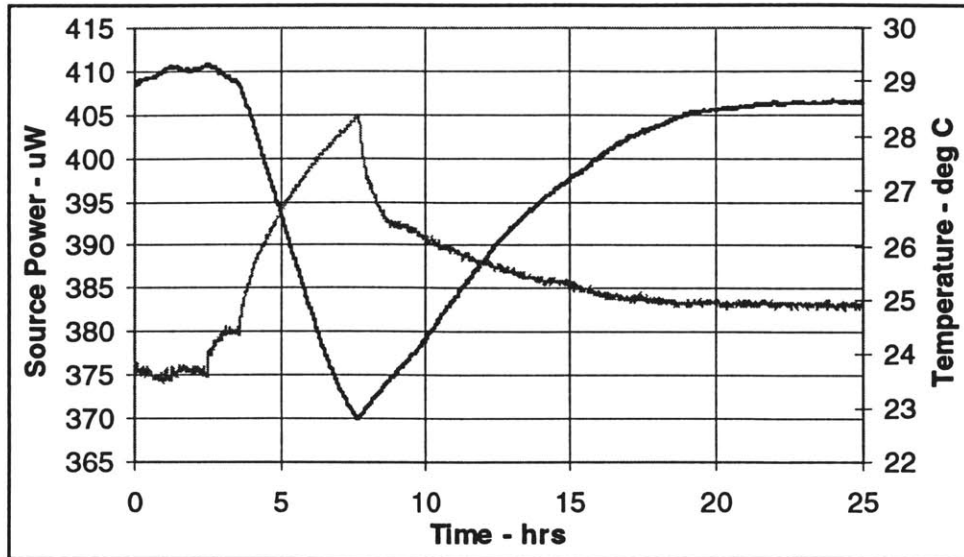
Figure 14: SLD Power and Temperature vs. Time. Black – Source Power; Grey – Temperature
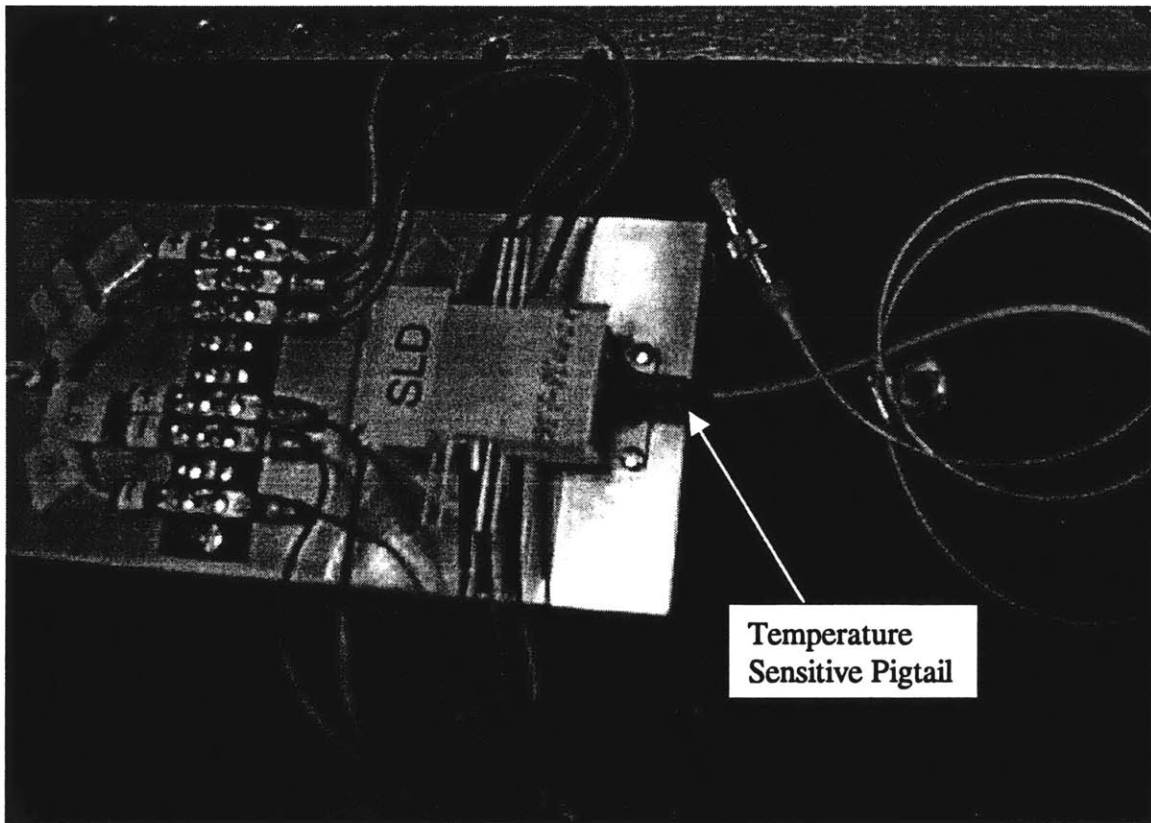
Figure 15: Photograph of high-powered SLD with exposed pigtail

Chapter 4   Components

4.1   Superluminescent Diode

In order to have a well-behaved gyroscope, a broadband source with a high output power is desirable. A broadband source is needed so that the coherence length of the output light is very short. This destroys the interference contrast of parasitic waves caused by backreflection, backscattering, and polarization cross coupling within the sensor coil.

An Anritsu superluminescent diode (SLD) operating at 1550 nm wavelength was employed. It was temperature stabilized using a temperature control unit produced by ILX Lightwave Corporation, providing temperature stability of 0.1 °C. The output power of the SLD should be above 1 mW for adequate power at the detectors. A nominal operating current is 125 mA, which gives an optical output of 1 mW. Figure 16 shows the SLD output versus current level when measured with a FC connector at the end of the fiber pigtail. If the source is spliced into the system, the output power is expected to increase because of the decreased loss through the interface.

The spectrum of the SLD was measured using a HP optical spectrum analyzer to characterize the full width at half maximum. The measured spectrum is shown in Figure 17. This measurement is used to calculate the coherence length, L_c, and the relative intensity noise, RIN, of the source

$$L_c = \frac{\lambda^2}{\Delta \lambda} \tag{12}$$

$$RIN = \sqrt{\frac{\lambda^2}{2\,c\,\Delta\lambda}} \tag{13}$$

where λ is the center wavelength of the source. The 3 dB bandwidth was measured to be 64.8 nm when the driving current is 125 mA. This leads to a coherence length of 37.1 μm and a RIN noise of 2.49E-7 rad/rt-Hz.

The coherence ripple of the source, measured in Figure 18, is the self-modulation
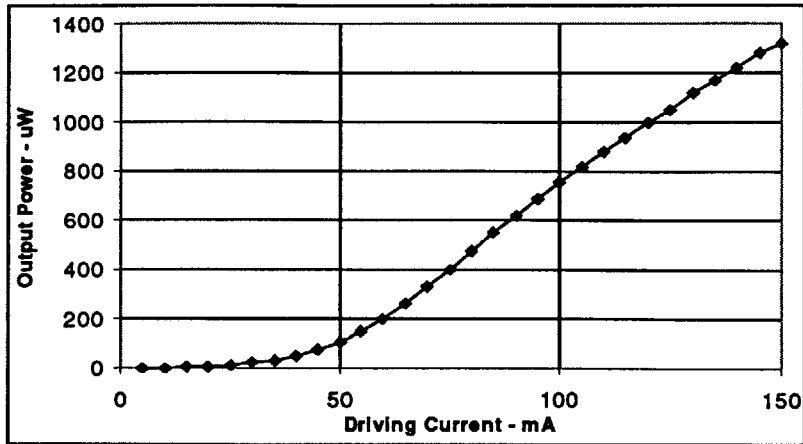
Figure 16: SLD Output Power vs. Driving
Current Curve
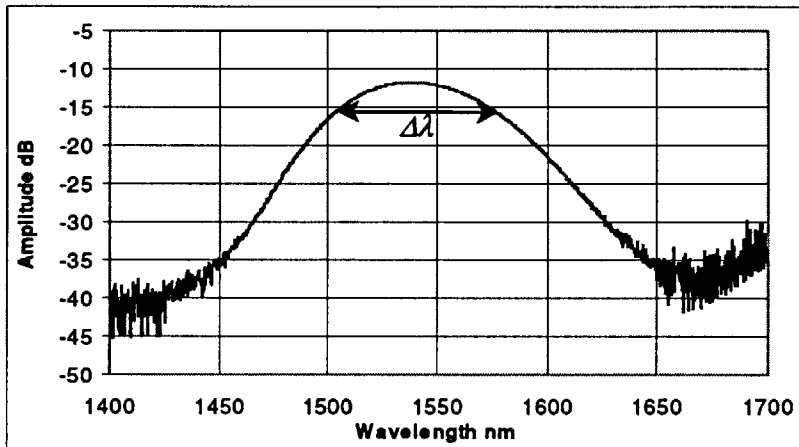
Figure 17: SLD Spectrum
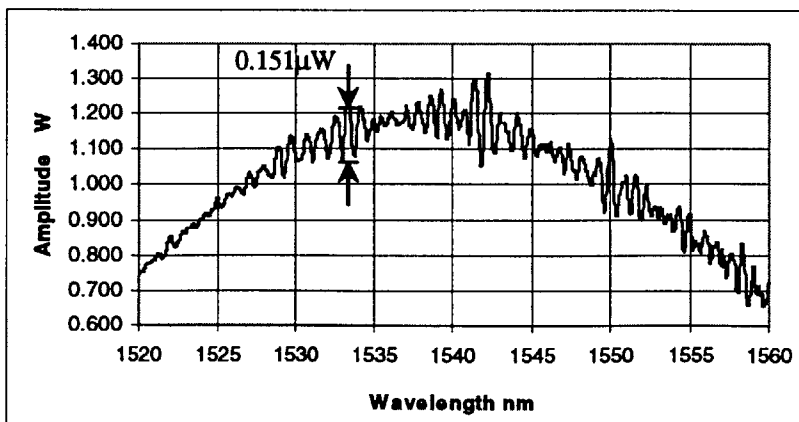
Figure 18: SLD Spectral Ripple

28

of the SLD spectrum due to backreflections into the resonant cavity. This can be caused by backreflections from the interface of splices or connectors. This value has an effect upon the gyroscope bias due to the Kerr Effect, which can be seen in Appendix A. This value is calculated by taking the ratio of the ripple to the maximum amplitude of the spectrum. The measured 1σ spectral ripple is 2.1%.
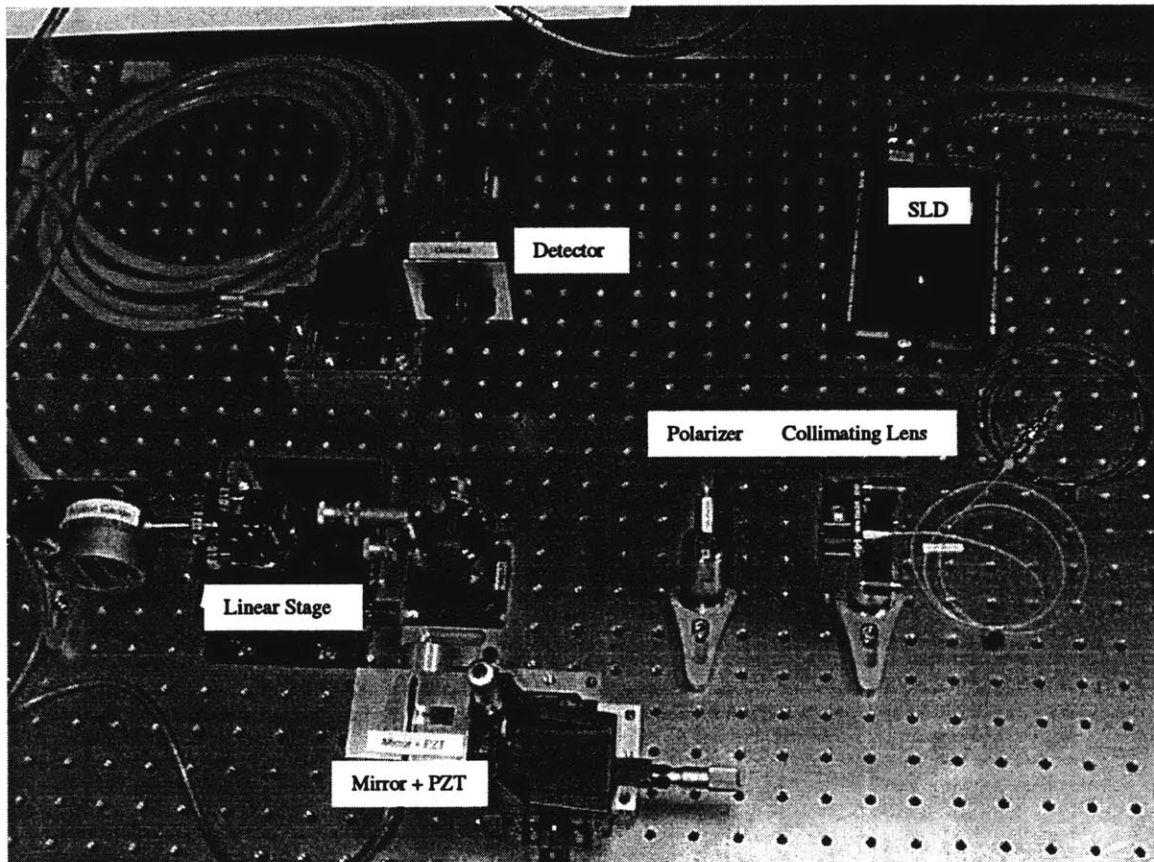
Figure 19: Photograph of Apparatus for Measuring Spectral Ripple of SLD; Consists of a Michelson Interferometer

4.2 Recirculator

As mentioned in Section 4.1, the SLD must be isolated from optical back reflections, as they induce spectral ripple and degrade system performance. It is also important to have as broadband a source as possible. However, it is difficult to find commercial optical isolators that have a flat passband over the entire bandwidth of 65 nm. It has been found that a recirculator can be used to isolate the source from back reflections. This device does have a relatively flat response over a wide wavelength range, providing 60 dB of isolation, while maintaining a low insertion loss of 0.8 dB.

The isolation is achieved by using two polarizers and a Faraday rotator. The input beam passes through a polarizer and becomes linearly polarized. The Faraday rotator rotates the beam 45°, then the light passes through the second polarizer, which is oriented 45° with respect to the first one. However, if light is entering from the opposite direction, it is rotated 45° such that its polarization is perpendicular to the polarized transmission axis. In this way the back reflected light is attenuated 60 dB. The JDS recirculator used is pigtailed to PM fiber at all ports.

4.3 Silicon Prism

The Si Prism, shown in Figure 20, is designed so that there is no material between the beam splitting point and the detector. By having it at Brewster's angle, it acts like a special polarizing beamsplitter, splitting the TE polarization approximately equally between the reflected and transmitted ports, but only transmitting the TM polarization. The measured transmittance of the polarizations is plotted in Figure 21. The prism is not perfectly anti-reflection coated, reflecting about 26 percent in power. These reflections cause increased loss in the OPFOG.
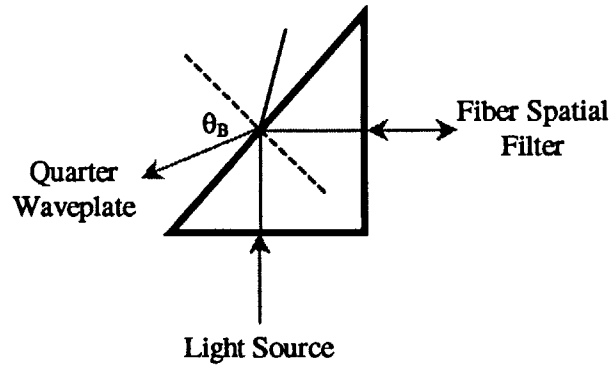
Figure 20: Design of Si Prism at Brewster's Angle
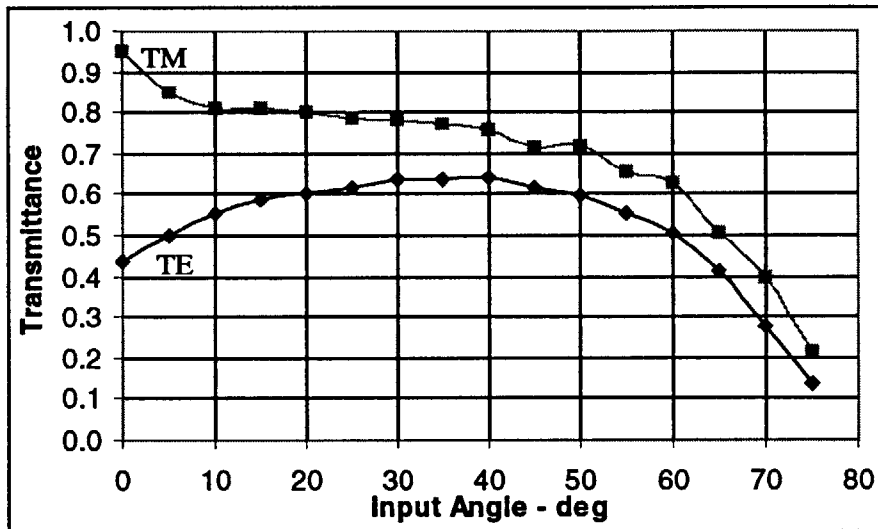
Figure 21: Si Prism Transmittance vs. Input Angle

The Si prism has an advantage in that it does not introduce a relative phase delay between the two polarizations. The prism has very little wavelength sensitivity, but the output beam direction changes with wavelength. There is also a dependence between input angle and output direction.

This directional change could cause difficulties in coupling into the PM spatial filter and detectors. By using Snell's Law, the output angle can be calculated. For a prism with an index of refraction of 3.49 and a rotational stage stability of 0.1°, the output

31

beam can move ± 0.35°. This should not cause a coupling problem into the detectors because they have a large active area.

4.4 Polarizing Beamsplitter

The polarizing beamsplitter (PBS) used for coupling into and out of the fiber coil is an ETEK custom pigtailed package. The package contains a PBS and three pigtailed ports with angle polished (APC) connectors on the fiber. The axis of the PM fiber must be oriented with the slow axis parallel to the polarization mode of the port. Otherwise, the OPFOG will not operate properly. The schematic of the PBS used is shown in Figure 22. The beamsplitter was mounted inside of the coil, being careful that the two output port fibers were in close proximity, so that temperature gradients would not cause birefringence variations in only one fiber.
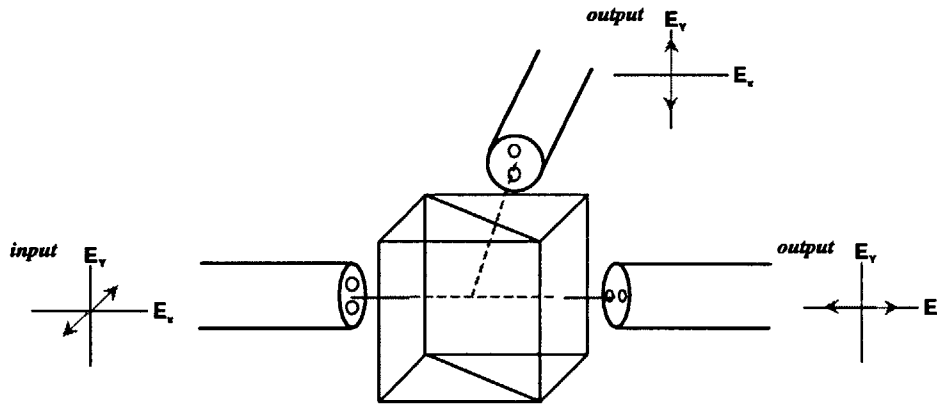
Figure 22: Pigtailed PBS Schematic

The splitting ratio of the beamsplitter is optimally 50-50 when light polarized at 45° is launched into the fiber. However, at room temperature it was measured to be 44-45.6 split with a 0.8dB insertion loss. This results in a nominal splitting constant, k_s, of 0.491. The splitting ratio changes with temperature 0.08 % /°C as outlined in Section 3.2. The splitting ratio error effects the bias due to the optical Kerr Effect, calculated to be 1.4E-5 deg/hr for the splitting constant given above.

4.5 Fiber Sensor Coil

The fiber on the coil is a polarization maintaining single mode fiber. The fiber coil is 6.8-inches in diameter wound upon a titanium mandrel. A titanium mandrel is used because it has an index of thermal expansion similar to that of the fiber. This reduces the amount of thermally induced mechanical stress upon the fiber, which may degrade its performance. Mechanical stresses and temperature fluctuations induce variations in the birefringence of the fiber, resulting in unpredictable polarization drift in the system. The coil was characterized for extinction ratio, which measures how well the coil preserves the input polarization state. It was measured to be 36.6 dB with an insertion loss of 1.6 dB.

The fiber coil was also potted to reduce acoustic and vibrational sensitivities in the instrument. The coil is encapsulated in an epoxy that is matched to the thermal expansion and mechanical properties of the fiber. The epoxy absorbs the vibrations and maintains the integrity of the fiber position locked in by the winding process. Without the epoxy encapsulation the gyroscope output will reflect the vibrations in the surrounding area, including people talking.

The wind of the fiber upon the mandrel is important to reduce thermally induced birefringence changes that may decrease the reciprocity of the instrument. Ideally, opposite ends of the fiber should be adjacent in the winding pattern so that both ends of the fiber will experience the same thermal gradients at the same time. There are different winding patterns that can accomplish this, like quadrapole winding, octopole winding, and hybrids of these and other schemes. The coil used in the OPFOG is quadrapole wound, which reduces the thermal sensitivity of the gyroscope well.

Rayleigh backscattering is reflections off of the fiber core that travel back towards its source. This causes a bias when the forward beam and backscattered wave are coherent with one another, producing an error in the detected rate of the gyroscope. The bias [9] due to this effect, $\Omega_{rayleigh}$, is

$$\Omega_{rayleigh} = K\ (1-2\ k_s)\sqrt{\frac{\lambda L_c S\ \alpha_r T_r B}{2\ n_{core}}} \qquad (14)$$

where K is the gyroscope scale factor, k_s is the beamsplitter split ratio, λ is the source wavelength, L_c is the coherence length of the source, S is the backscattering factor, α_r is the Rayleigh scattering coefficient, T_r is the coherence time of Rayleigh scattered phase, B is the bandwidth, and n_{core} is the index of refraction of the fiber core. Using the parameters listed in Appendix A, the Rayleigh bias for this instrument is 0.034 deg/hr.
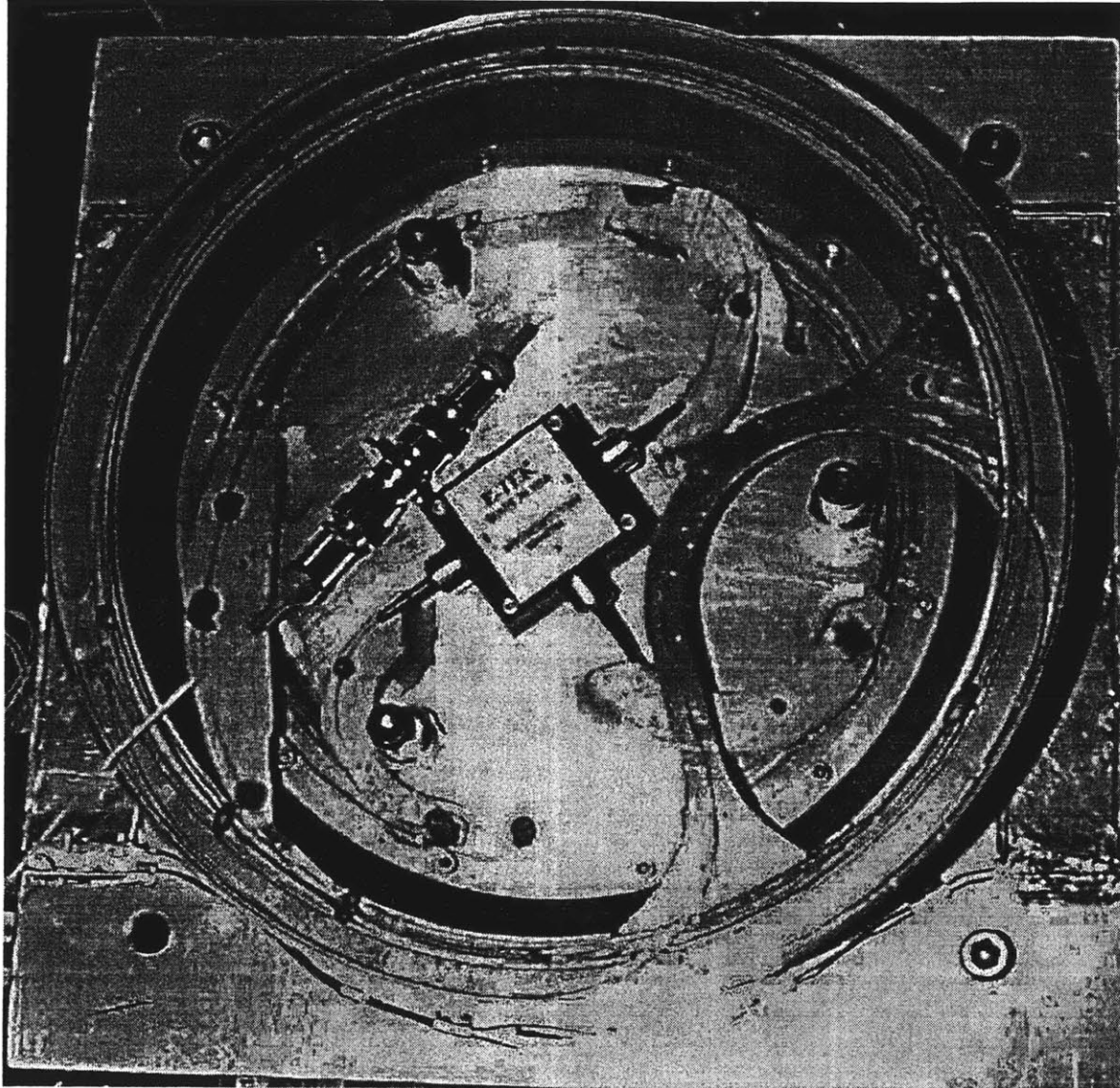
Figure 23: Photograph of Coil Assembly

4.6   Plate Beamsplitter

For the plate beamsplitter a microscope slide cover was used. This component was chosen because it is extremely thin, causing little difference between the signal and monitor paths. The reflection from the face provides a 15-83 percent split with an insertion loss of 0.1 dB. This provides ample signal to the detectors to implement the temperature-monitoring scheme proposed.

4.7   Detector

The detectors are Epitaxx 3mm diameter InGaAs detectors with responsivities matched to within 2%. Large area free space detectors were chosen so that the signal beams would not have to be focused down into a fiber. If it were focused into a fiber, some signal would be lost through the coupling, and the system now depends upon mechanical alignment stability. By using a large active area, the alignment can shift slightly, and the optical signal would still be detected, whereas with a fiber pigtailed detector, the focused beam would "walk off" the fiber core causing errors in the detected signal.

The shot noise, I_{Shot}, is the fundamental limit of the detectors. It is caused by photons creating electron-hole pairs, which translate into current.

$$I_{Shot} = 2\ e\sqrt{\frac{2\ \eta\ \lambda\ B\ P_{det}}{h\ c}} \tag{15}$$

where η is the detector quantum efficiency, λ is the source wavelength, B is the bandwidth of the receiver, P_{det} is the incident power upon the detector, and h is Plank's constant. A factor of 2 is added in the calculation of the shot noise to account for both detectors in the balanced detector circuit. Using a quantum efficiency of 0.88, bandwidth of 2.6 MHz and an incident power of 30 μW, the shot noise of the balanced detector is 26.3 nA.

Johnson Noise arises from thermal fluctuations in the load resistor of the photodetector. The thermal energy from the resistor allows electrons to move randomly, causing a random current, I_J.

$$I_J = \sqrt{\frac{4\,k_B T\,B}{R_L}} \tag{16}$$

where k_B is the Boltzmann's constant, B is the bandwidth of the reciever, T is the temperature, and R_L is the load resistor. For an operating temperature of 50 °C, detector bandwidth of 2.6 MHz, and a load resistor of 10 MΩ, the Johnson noise is 68.1 pA.

The noise equivalent power, NEP, is the amount of incident power for which the signal-to-noise ratio of the detector is unity.

$$NEP = \frac{I_{total}}{\rho} \tag{17}$$

where ρ is the responsivity of the detector. It is therefore the minimum detectable power on the detector. For a responsivity of 0.95 A/W, the minimum detectable power is 27.7 nW.

4.8 Electronics

The electronics consisted of a balanced detector circuit with summing and differencing nodes. A shunt feedback configuration [8] could not be used because access to both detector signals is necessary to implement an output ratio, as mentioned above. Instead, a trans-impedance amplifier with a gain of 3E5 is used for each diode, followed by a sum and difference circuit. The electronics are shown in Figure 24.

36
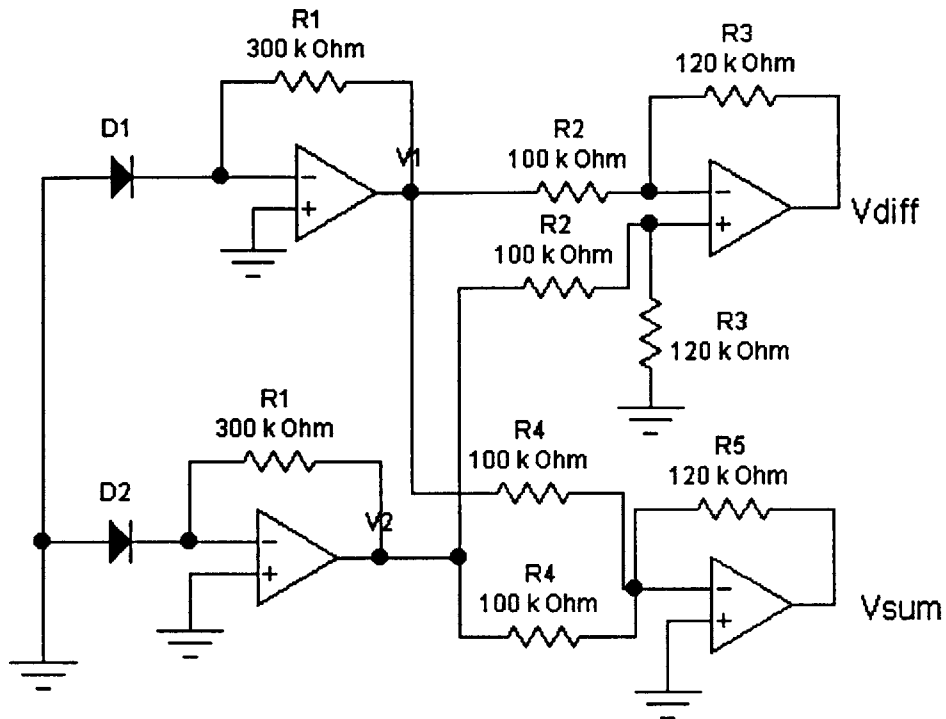
Figure 24: Balanced Detector Trans-Impedance Amplifier Circuit. The two diodes are the photodetectors.

For detectors with responsivity, ρ, and incident power, P, the output current of the photo-detector is I.

$$I_1 = \rho \, P_1 \tag{18}$$

$$I_2 = \rho \, P_2 \tag{19}$$

After the trans-impedance amplifier, the voltage at nodes *V1* and *V2*, respectively, are

$$V_1 = R_1 I_1 \tag{20}$$

$$V_2 = R_1 I_2 \tag{21}$$

The output of the differencing circuit, V_{diff} is

$$V_{diff} = -\frac{R_3}{R_2}(V_1 - V_2) \tag{22}$$

The output of the summing amplifier, V_{sum} is

$$V_{sum} = -\frac{R_5}{R_4}(V_1 + V_2) \qquad (23)$$

By substitution into equations 21 and 22, V_{diff} and V_{sum} are

$$V_{diff} = -\frac{R_1 R_3 \rho}{R_2}(P_1 - P_2) \qquad (24)$$

$$V_{sum} = -\frac{R_1 R_5 \rho}{R_4}(P_1 + P_2) \qquad (25)$$

Therefore, the output ratio of the difference and sum, V_{ratio} is proportional to the ratio of the difference and the sum of the detector power.

$$V_{ratio} = \frac{R_3 R_4}{R_2 R_5} \cdot \frac{P_1 - P_2}{P_1 + P_2} \qquad (26)$$

By using the selected resistor values the output ratio becomes

$$V_{ratio} = \frac{P_1 - P_2}{P_1 + P_2} \qquad (27)$$

High precision resistors with tolerances of 0.1% are used for resistors $R1$ to ensure that excess noise is not added to the system when the diode signals were being amplified.

4.9 Connections

All of the connections between the fiber to fiber interfaces are angle polished connectors at 10°. This reduces the backreflections that are coupled back into the fiber to less than 4%. The two connections between the ETEK beamsplitter to the fiber coil are spliced together in order to achieve the best alignment between the polarization axes.

Chapter 5   Analysis

5.1   Power Budget

Using Doerr's OPFOG configuration and an input power of 1 mW, an estimated 18.1 dB loss through the system would yield a total output power at the detectors of 15.5 µW. The power estimates and measured component losses are shown in Table 1. In the actual system at rest, there is 16.8 dB of loss resulting in a power of 10.5 µW to each detector.

Element	Estimate	Measured
Recirculator (linearly pol. light)	0.80 dB	0.40 dB
Polarizer	0.80 dB	0.71 dB
Plate Beamsplitter	0.10 dB	0.09 dB
Half Waveplate	0.10 dB	0.06 dB
Prism Reflection	5.50 dB	5.2 dB
ETEK Beamsplitter	1.00 dB * 2	0.95 dB *2
Coil	1.60 dB	1.60 dB
Prism Transmission	3.60 dB	3.60 dB
Quarter Waveplate	0.10 dB	0.06 dB
Wollaston Prism	0.50 dB	0.53 dB
Collimating Lens	1.0 dB * 3	0.83 dB * 3
TOTAL	**18.10 dB**	**16.64 dB**

Table 1: System Power Loss

However, when the temperature-monitored configuration of Figure 5 is implemented, losses in the system are significantly higher. The original temperature monitoring system, shown in Figure 25, employed the use of two polarizers to obtain the correct polarizations for the signal and monitor beams. The output of the SLD is primarily linearly polarized (85% in one polarization). A quarter waveplate is used to circularly

polarize the light, which is then split into a signal and monitor path. The signal path requires light polarized vertically. However, the monitor path requires light polarized at 45° in order to probe the biasing quarter waveplate. By using a quarter waveplate to create circularly polarized light, both polarizations can be made. The polarizers produce the appropriate polarization, but this implementation adds an extra 3 dB of loss through the system.

Another scheme, shown in Figure 26, was implemented to eliminate the excess loss. This implementation uses two half waveplates to rotate the polarization, resulting in a significantly smaller insertion loss. A polarizer filters the SLD output to produce linearly polarized light, which then passes through the plate beamsplitter. The signal branch passes through a half waveplate oriented at 0°, thus passing though without changing the polarization. The monitor branch passes through a half waveplate oriented at 22.5°, rotating the polarization by 45°. The insertion loss of this is significantly less, losing only 0.1 dB through the half waveplates. The second method was implemented for the temperature monitored OPFOG.

Si Prism @
Brewster's angle θ_B

to Fiber
Sensor Coil

to
Detectors

Mirror

θ_B

in

out

Polarizer
@ 45°

Polarizer

Mirror

Plate BS

λ/4 Plate
@ 45°
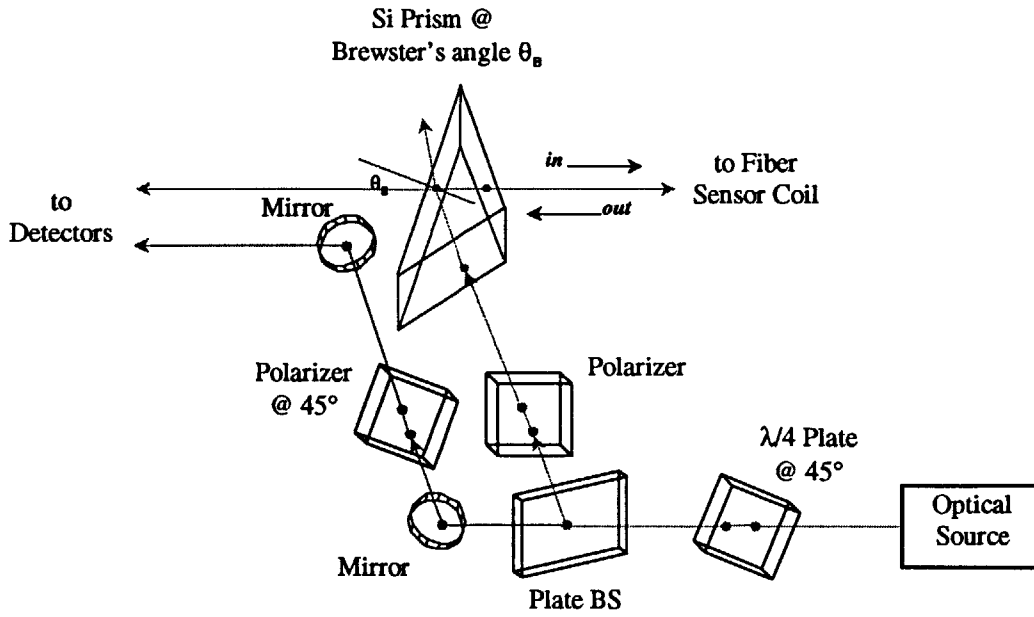
Optical
Source

Figure 25: Optical Input Train for Signal and
Monitoring Paths

Si Prism @
Brewster's angle θ_B

to Fiber
Sensor Coil

to
Detectors

Mirror

θ_B

in

out

λ/2 Plate
@ 22.5°

λ/2 Plate

Mirror

Plate BS

Polarizer
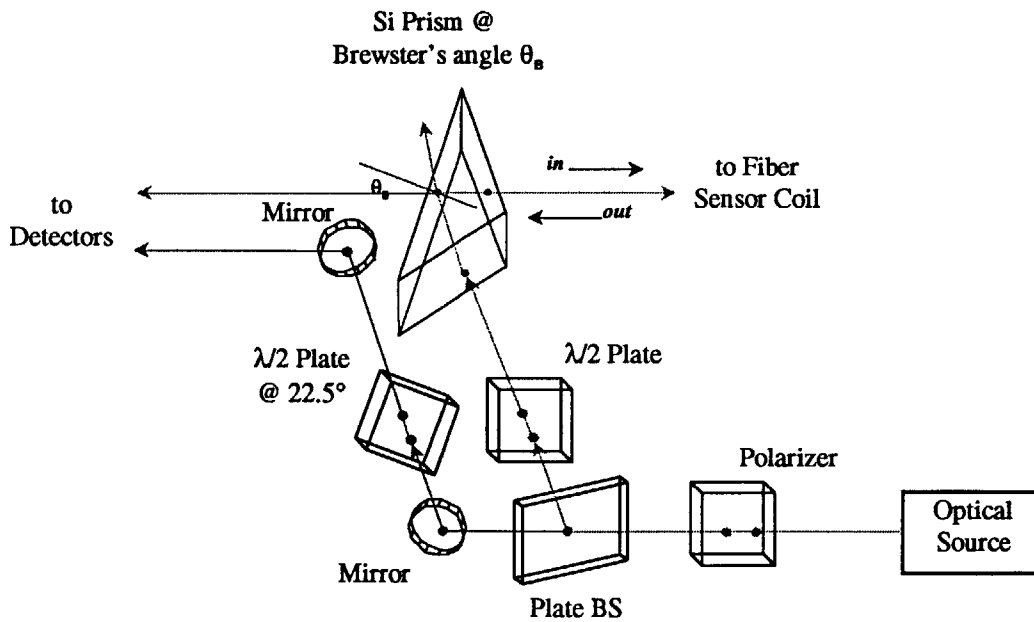
Optical
Source

Figure 26: Improved Optical Input Train

41

5.2 Bias Analysis due to Polarization

The bias analysis performed in Mathcad, detailed in Appendix A, followed an approach presented by Kintner [10] to examine the bias error due to polarization. The analysis used to calculate the bias drift of the standard fiber optic gyroscope could not be directly used because of the different configuration of the polarization axes of the fiber. Kintner unfolded the gyroscope into two fiber delay lines connected at the ends by the beamsplitter. By calculating the total effective polarization filtering through the system, the bias error due to polarization crosstalk in the system can be estimated.

The crosstalk values used in this estimate were very conservative. The conventional gyroscope contains an IOC that polarizes light extremely well. The OPFOG configuration provides most of its polarization filtering through the polarizing beamsplitter, which is traversed twice, effectively doubling its filtering capacity. By using conservative 30 dB polarization control of the input beam, and −28 dB for the beamsplitter extinction ratio, a gyro bias error of 5.2E-3 deg/hr can be expected.

By using active alignment for the launch polarization with the beamsplitter axis, 35 dB polarization control can be obtained for the input beam. It is also possible to purchase polarizing beamsplitters with more than −30 dB extinction between the polarization axes. With the more rigorous polarization constraints, a 1σ gyroscope bias of 7.4E-4 deg/hr can be realized. A similar conventional gyroscope with an IOC polarization filtering of −70 dB and a launch of −30 dB yields a gyro bias of 1.1E-3 deg/hr.

5.3 Minimum Detectable Rotation Rate

The minimum detectable rotation rate is calculated to characterize the best performance that can be expected from the instrument. The total noise, N_T, of the system is the root sum of the squares of the RIN, Shot noise, Johnson noise, and thermal noise.

$$N_T = \sqrt{RIN^2 + I_{Shot}^2 + I_J^2} \qquad (28)$$

42

which leads to a total noise of 8.87E-8 rad/rt-Hz and a minimum detectable rotation rate of 2.3E-2 deg/hr. For a similar conventional gyroscope, the minimum detectable rotation rate is 3.8E-2 deg/hr.

5.4 Scale Factor Errors

The scale factor of the gyroscope will change due to changes in the coil diameter, the length of the fiber, and source wavelength fluctuations. The sensitivity to each of these errors is found by differentiating the gyroscope scale factor with respect to each of these terms. This gives an error of 5.4E-5 ppm due to diameter changes, 9.3E-9 ppm due to fiber length variations, and 4.5 ppm due to source center wavelength fluctuations. This leads to a total 4.5 ppm scale factor change for the OPFOG or conventional gyroscope with the same source and sensor coil. This calculation is carried out in detail in Appendix A.

The biasing quarter waveplate will add an error to the scale factor when the source center wavelength varies and when the temperature changes. The added scale factor error, SF_{qwpT}, will vary in a sinusoidal fashion.

$$SF_{qwpT} = \sin(\alpha\, \Delta T) \tag{29}$$

where α is the temperature coefficient of the waveplate and ΔT is the temperature control of the gyroscope. For the measured waveplate coefficient of 6.47E-4 rad/°C and a temperature control of 0.1 °C, the scale factor error will be 64.7 ppm.

When the source center wavelength changes, the scale factor error, $SF_{swq\lambda}$, will also change in a sinusoidal manner.

$$SF_{qwp\lambda} = \sin(\pi/2 \; \lambda_c) \tag{30}$$

where λ_c is the source wavelength stability. If the wavelength is controlled to 1 ppm, the resulting scale factor error is 1.6 ppm. Altogether, the waveplate adds a total scale factor error of 64.7 ppm.

5.5 Magnetic Faraday Errors

The magneto-optic Faraday effect is caused by a longitudinal magnetic field changing the polarization of the light wave by the Verdet coefficient of the medium, in this case the optical fiber. In a fiber ring, it will manifest itself as a phase difference, $\Delta\theta_F$, in the counter-propagating waves, causing a false rotation rate in the gyroscope output [11,12].

$$\Delta\theta_F = \frac{4\,V\,B\,D}{\Delta\beta}\sqrt{2\,\pi\,N\,W_f} \qquad (31)$$

where V is the Verdet coefficient of the fiber, B is the applied magnetic field, D is the diameter of the coil, $\Delta\beta$ is the difference in propagation constants of the fiber axes, N is the number of turns in the coil, and W_f is the spectral twist characteristic of the fiber coil. From the Earth's magnetic field, a phase difference of 15 μrad causes a bias of 0.013 deg/hr in the tested gyroscope. However, other sources of magnetic radiation can cause higher drift in the instrument due to the Faraday effect.

Typically, a μ - metal shield is used to reduce the bias error from the Faraday effect. This shield is composed of high permeability metal that blocks the magnetic radiation from the sensing coil. This can result in a reduction of the error by one or two orders of magnitude.

Another method of reducing this error source is controlling the spectral twist of the fiber as it is wound upon the mandrel. As PM fibers are manufactured, the fiber is drawn from a silica preform into long optical fibers. As the fiber is pulled, the stress member will twist slightly within the cladding, resulting in a twist spectrum that is built in during the manufacturing process. There is an additional twist element added when the fiber is wound upon a take-up spool or coil mandrel. Usually, the fiber is not wound such that the stress member is oriented in the same direction during the wind. The fiber is allowed to twist of its own accord when made into a coil. However, if the stress member were monitored during the winding process such that the twist was minimized, the total twist in the fiber coil would be limited by the twist frozen into the fiber during

manufacturing and the gyroscope error due to the Faraday effect would be significantly reduced.

Chapter 6   OPFOG Data

Gyroscope performance can be characterized by several parameters, angle random walk, bias drift and scale factor stability. Angle random walk is the short term random fluctuations that are caused by white noise, like shot noise, source relative intensity noise (RIN), and mechanical and acoustical vibrations. Angle random walk is typically measured in deg/rt-hr. Bias drift is the long term peak-to-peak variation of the mean value of the output signal. Thermal variations and mechanical alignment drifts cause the long-term drift, which is usually measured in ± deg/hr. For a fiber gyroscope, the scale factor has to be accurate to measure high rates of rotation. For inertial grade instruments, an angle random walk of less than 0.001 deg/rt-hr, a bias drift of less than 0.01 deg/hr and a scale factor accuracy of less than 5 ppm need to be met [13].

6.1   Experiment

A gyroscope using the temperature monitored OPFOG scheme was constructed and tested. It was built according to Figure 5 with the improved optical input train of Figure 24. The components used are as described in Chapter 4. A photograph of the system a rate table is shown in Figure 27.

To calibrate the gyroscope, the optics and sensor ring were placed on a rotatable platform that has an angular velocity capable of micro-radian accuracy. The scale factor of the gyroscope was determined by rotating the table in one direction, then reversing the rotation and repeating to check for hysterisis.

To measure long-term stability, the coil assembly and optics were exposed to room temperature initially. Later they were placed into a large foam box to insulate the gyroscope from large thermal gradients. The output from the balanced detector was connected to a voltmeter and computer, which recorded the data.
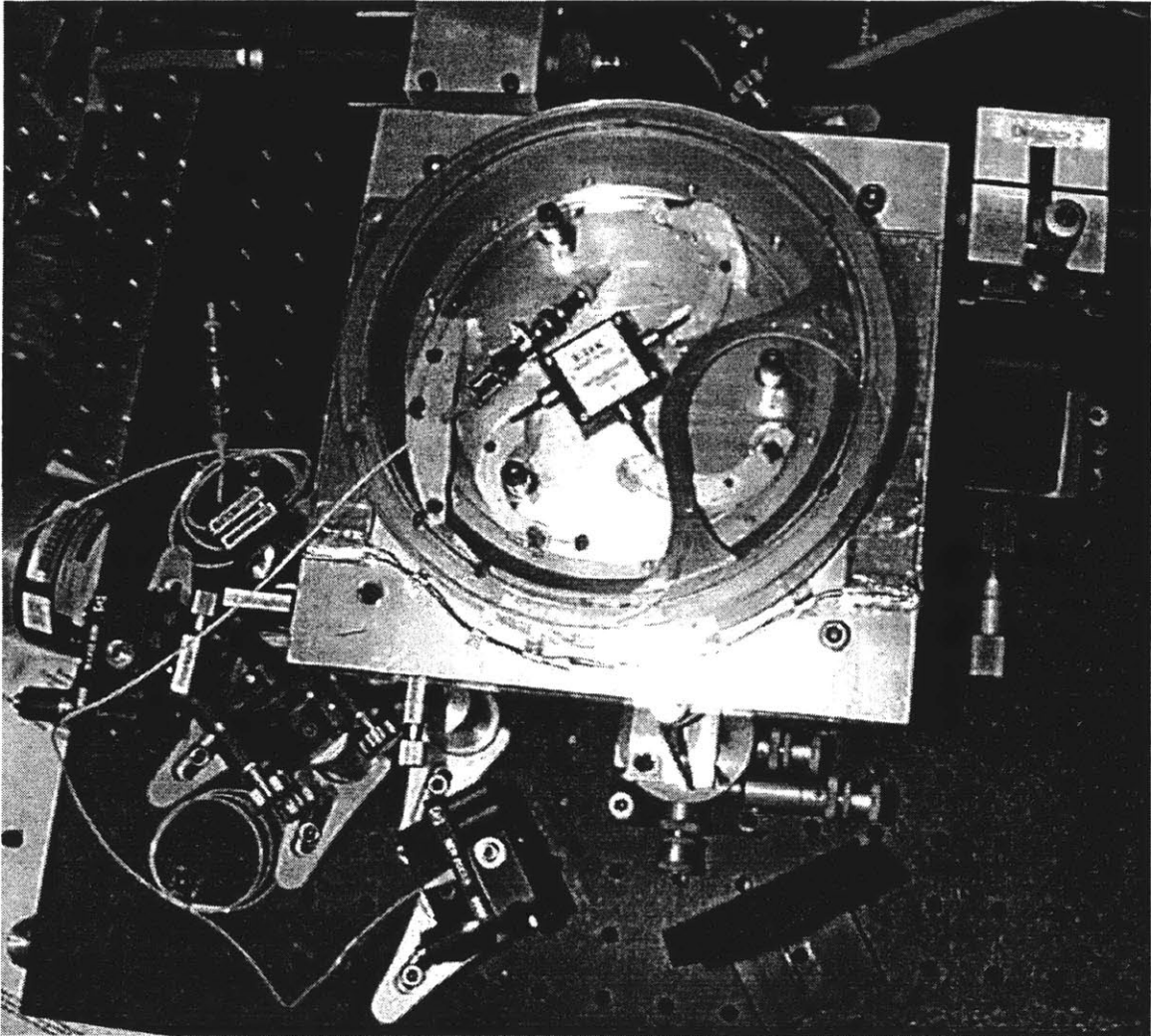
Figure 27: Photograph of OPFOG on rate table:
Coil is mounted on plate suspended above optics
to fit on 12" × 12" area

6.2   Scale Factor Measurement

The scale factor, SF, was determined by rotating the gyroscope at a velocity of 150 deg/hr clockwise for two minutes, then counter clockwise for two minutes. To check for instrument hysterisis the gyroscope was rotated clockwise again to make sure that the output signal returned to its original signal value.

$$SF = \frac{\Delta\Omega}{\Delta V} \qquad (32)$$

where $\Delta\Omega$ is the difference in the rotation rate and ΔV is the change in the gyroscope output signal.

The scale factor calibration data is shown in Figure 28. A change in the balanced detector output voltage of 10.55 mV was measured, resulting in a scale factor of 28.4 deg/hr /mV.
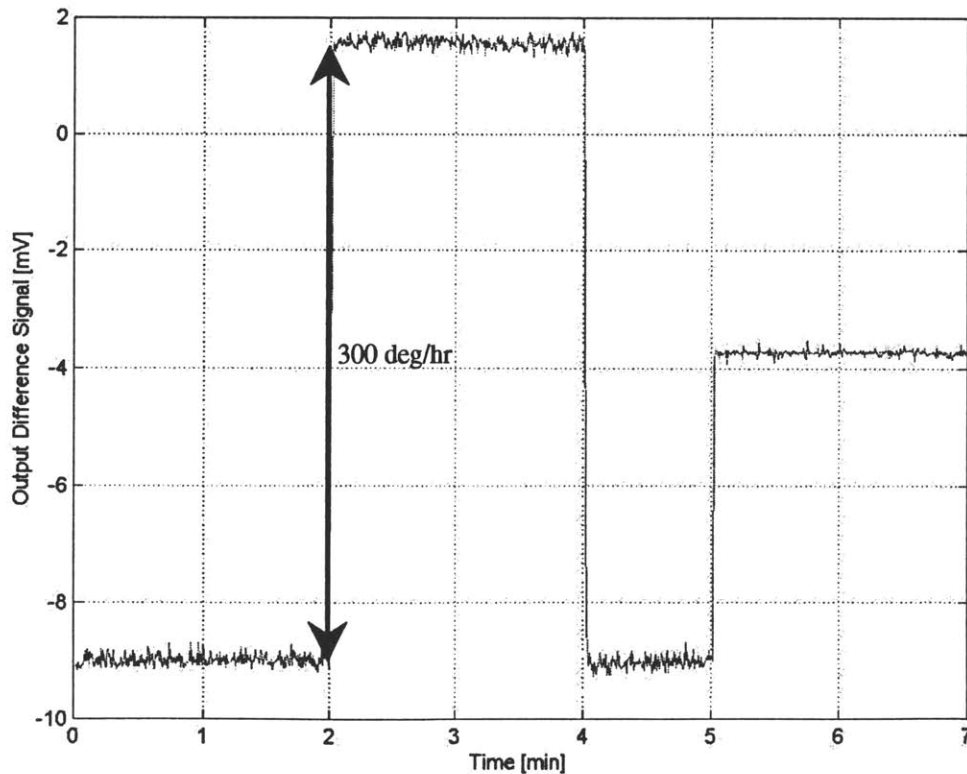
Figure 28: Scale Factor Calibration Data for Original OPFOG

48

6.3 Angle Random Walk

The angle random walk (ARW) of the instrument is measured from the last two minutes of the scale factor calibration, when the instrument is not under rotation. The high frequency jitter of the output is due to shot noise, RIN noise, mechanical vibrations from the room, and acoustical vibrations. Thermal variations do figure into the ARW because its low frequency nature.

$$ARW = \frac{\Delta\Omega_s}{6\sqrt{B}} \cdot \frac{1}{60}$$ (33)

where $\Delta\Omega_s$ is the measured peak-to-peak value of the high frequency gyroscope signal in deg/hr and B is the detection bandwidth in Hz. For a detection bandwidth of 10 Hz and a peak-to-peak jitter of 0.05 mV, the measured ARW is 1.2E-3 deg/rt-hr. The data set used is shown in Figure 29. The spikes in the data set are due to the vibration of the building, 15 Hz, leaking through to the instrument. These spikes were ignored when calculating the angle random walk value. The measurement was repeated with the long-term bias drift data and was found to be consistent with the above value.

The model predicted a value of 3.2E-4 deg/rt-hr. The discrepancies between the measured and predicted results come from a variety of sources. The RIN is not completely cancelled, as assumed in the model, because the detectors are not perfectly matched. There is more than just Johnson noise from the detector circuitry because a shunt configuration was not used, as discussed in Section 4.8. The mismatch of the trans-impedance resistors will add noise to the output.
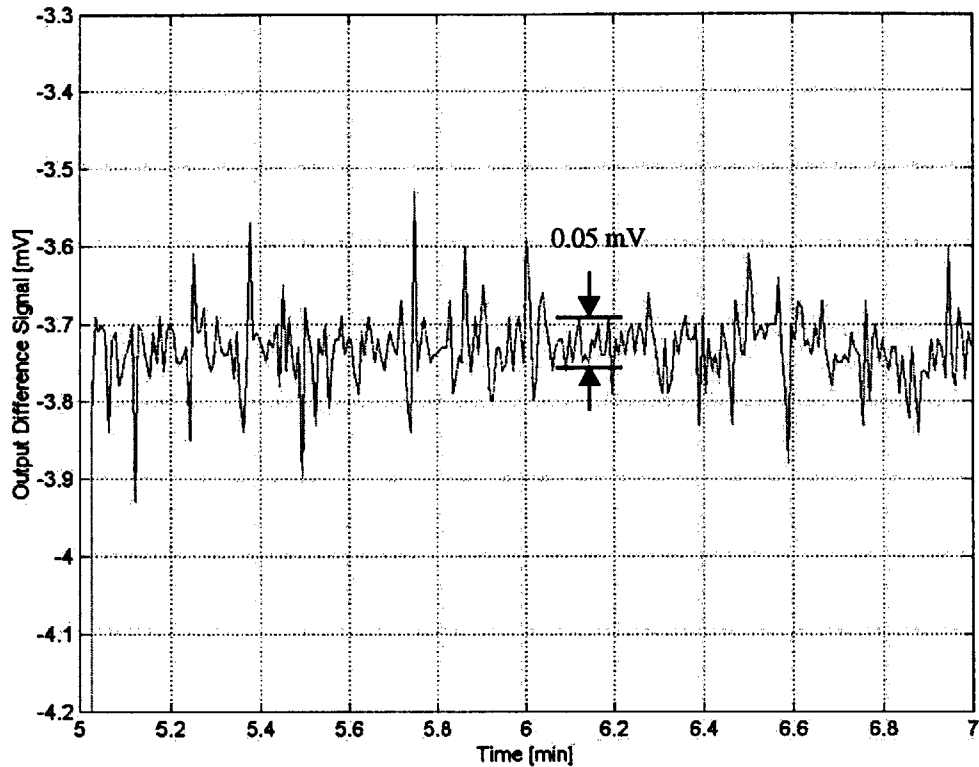
Figure 29: Angle Random Walk Data – exploded
view of last two minutes of Figure 28

6.4 Bias Drift

The bias drift data was taken overnight for a period of 13 hours. The usable area
of this data is in the middle of the night because that is when the thermal transients from
the air conditioning system die down. There is also no traffic in the lab causing vibrations
to the rate table. The data taken in Figure 30 was enclosed in an insulting foam box to
reduce air currents between the optical elements. The optics and sensing coil were
exposed to a temperature change of five degrees Celsius during the course of the night.

The 1σ bias drift is measured to be 1.1 deg/hr over a 3-hour interval and 0.33
deg/hr over a 15-minute interval. Doerr measured a peak-to-peak drift of 1.2 deg/hr over
a 15- minute interval. The model predicted a drift of 9E-4 deg/hr. A major source of drift
appears to be air turbulence in the bulk optics near the detectors. Another error is that the
coil assembly was not magnetically shielded. In order to get better performance, the

gyroscope should be enclosed in a μ-metal shield. Birefringence changes and splitting ratio change due to temperature in the ETEK polarizing beamsplitter also increase the drift.
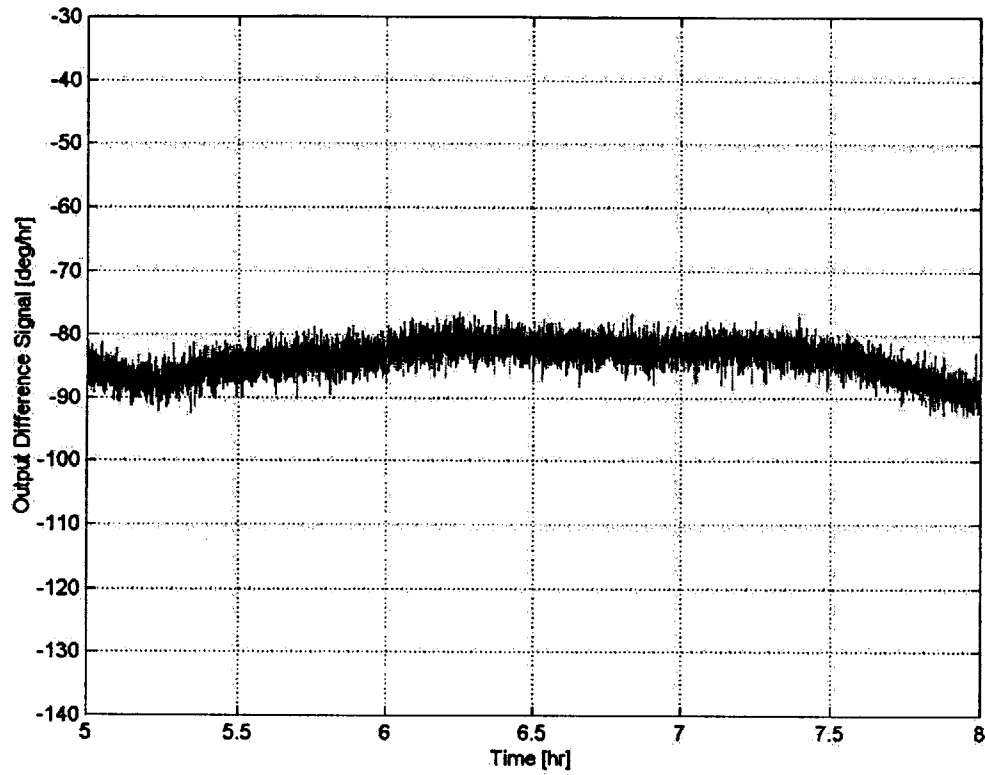
Figure 30: Bias Drift Data over 3 hours – starting around midnight

Chapter 7   Conclusions

7.1   OPFOG Advantages/Disadvantages

The IFOG has several disadvantages, such as high cost, complicated electronics, gyroscope drift, and a relatively large instrument size. This is driven by the high cost per unit length of PM fiber and the integrated optical circuit. The phase modulation needed to attain maximum sensitivity is provided by the IOC and often results in bias drift due to the instability of the $LiNbO_3$ crystal and requirements for the high frequency electronics to demodulate the output signal. To attain a large dynamic range, conventional gyroscopes operate closed loop, resulting in complex electronics. The length of the usually establishes the minimum size of the IFOG's fiber coil.

The OPFOG has several advantages over the conventional IFOG, listed in Table 2. The first is that the fiber coil, which can be reduced due to the absence of the IOC. The optical train is composed of bulk optical components, which can be miniaturized to fit into a reduced instrument diameter. The second advantage is that the balanced detection scheme effectively eliminates excess intensity noise from the source. The passive bias is introduced outside of the fiber ring, allowing for a medium dynamic range and simpler electronics. Lastly, this configuration allows us to use a squeezed light approach to reduce the noise below the shot noise limit [4].

The are also problems associated with the OPFOG. The dynamic range of the instrument is medium because the system is operating open loop. The output signal of the OPFOG is also intensity dependent. Since the OPFOG operates at baseband, it is subject to 1/f noise. All of the above issues can be addresses by digital post-processing or by feedback loops in the instrument.

	IFOG	OPFOG
Instrument Size	3"	< 2"
RIN Noise	Minimally reduced	Significantly reduced
Modulation	High frequency	No modulation
1/f Noise	Small due to modulation	Can be reduced by electronic chopping amplifier
Dynamic Range	Many orders of magnitude	Medium
Intensity Dependant	N/A	Can be eliminated by sum/difference approach
Squeezed Light	N/A	Can integrate into unused BS port

Table 2: Comparison between IFOG and OPFOG

7.2 Gyroscope Size

The major advantage to the OPFOG is that the gyroscope can be made relatively small compared to the conventional IFOG and still achieve similar performance. This is achieved because all of the optical components are bulk optic elements and can be machined using micro-mechanical methods upon one silica substrate.

The major limitation of all fiber optic gyroscopes is the fiber coil diameter. As the coil diameter decreases, there are more losses in the fiber and added birefringence induced by mechanical stresses will degrade the polarization maintaining properties of the PM fiber. The following is the theoretical limit of the minimum fiber optic coil size. There is a critical bend radius, Rc, of a fiber coil where optical losses sharply increase [14].

$$R_c = \frac{D_{core}}{2\ NA^2} \tag{34}$$

where D_{core} is the fiber core diameter and NA is the numerical aperture of the fiber. For a core diameter of 9 μm and a numerical aperture of 3.86E-2, the critical coil diameter is 6 mm. By allowing the fiber coil to be 2 inches in diameter, the insertion loss factor due to bending is small, and sufficient polarization extinction ratio exists to meet the performance

requirements. Sufficient space to insert all of the components into the center of the coil mandrel is also maintained, as shown in Figure 31.
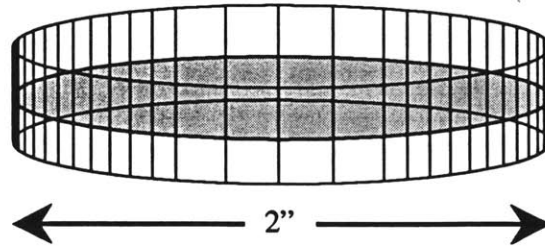
Figure 31: Schematic of gyroscope layout. Wire frame – fiber coil; shaded area – optical substrate with components

The shrinking of the coil diameter will allow the overall OPFOG size to be just over 2 inches in diameter. The conventional gyroscope has a size limitation of approximately 4 inches in diameter due to the size of the IOC, its biasing element. The IOC needs to be about 2 inches long in order to achieve the necessary polarization filtering level needed by the conventional IFOG.

7.3 Squeezed Light

To eliminate quantum-mechanical noise, quadrature squeezing can be utilized, where a squeezed vacuum is injected into an empty port of the gyroscope interferometer. By using either photon-number squeezing or quadrature squeezed light, the output noise of the instrument can be more than 3 dB below the shot noise limit. But this will only work for balanced detection, as in the OPFOG. The conventional IFOG does not use true balanced detection, and consequently cannot employ squeezed light technology.

7.4 Dynamic Range

The dynamic range of the OPFOG is medium because the instrument is operating open loop and needs to be closed either by digital post-processing or a waveplate feedback loop in order to achieve sufficient dynamic range. Since the output signal is

54

sinusoidally dependent upon the rotation rate, small rotation rates are measured very accurately. However, large rotation rates will be in a very low sensitivity bias point. The IFOG overcomes this failing by operating closed loop, adjusting the bias so that no matter what the rotation the instrument is always at a high sensitivity bias point. This method can also be applied to the OPFOG with a variable retardation plate that can provide a nominal bias of $\pi/2$ and will vary linearly around this point.

A second method is to close the loop digitally by using a high speed digital processor. A third approach would be to mount a micro-mechanical gyroscope that measures relatively high rotation rates within the OPFOG. The OPFOG would be used to measure low rotation rate, and the mechanical gyroscope to measure high rates. By switching between the two, and instrument with a large dynamic range can be built.

7.5 Output Intensity Dependence

As discussed in Section 3.3, the stability of the scale factor of the instrument is dependent upon the source intensity stability. As the scale factor changes, so does the measured rotation. One way to eliminate this phenomenon is to measure the intensity at the output, then divide it out of your output signal. This is practically done by taking the ratio of the difference and sum of the detectors. A drawback to this configuration is that it may reintroduces the excess intensity noise that was eliminated by balanced detection if not properly processed. While the system has noise sources, the excess noise in not dominant. However, as the noise floor approaches the shot noise limit, it will become a major source of noise in the system, limiting the resolution of the gyroscope. If this is the case, a control loop will have to be added to stabilize the source intensity.

7.6 Instrument Modulation

The OPFOG operates at baseband. While this eliminates the need for complicated high frequency electronics to demodulate the output signal, it makes the system susceptible to 1/f noise. This could be eliminated by modulating the signal before it reaches the detector, after it is detected, or at the source. The signal could be chopped

55

optically before it reaches the detectors to modulate the signal and move it away from baseband. Or, the signal could be chopped digitally within the electronics after it has been detected. Lastly, a pulsed source could be used to provide the modulation. The modulation carrier frequency would not have to be high, on the order of 10 kHz, to significantly reduce the 1/f noise in the system.

7.7 Recommendations

By developing a method to accurately align the polarizations of the optical components, the current system can be miniaturized. A first step would be to build the system using half-inch diameter bulk components upon a stable substrate or in a tube to ease alignment. The miniaturized optics would ideally be contained within an inch and a half diameter circle. This would allow development and test of a two-inch diameter coil. The next step is to micro-machine the optical elements into a piece of silica, such that alignment issues are taken care of when the components are machined. At this point, integration into a viable gyroscope should be relatively simple.

A pulsed source with an intensity control loop should be used to reduce the 1/f noise of a baseband instrument. With the intensity control loop, simple balanced detection will eliminate excess intensity noise, while allowing the possibility of squeezing the light to reduce the output noise below the shot noise limit.

The coil assembly should be magnetically shielded to reduce errors due to the Faraday effect. The gyroscope should be enclosed to reduce air currents between the optics and temperature controlled to reduce the thermally induced errors in the coil. By performing these improvements, the bias drift of the instrument should decrease even more than was shown in this thesis.

References

[1] H. Kajioka, "Optical fiber laser gyroscope," *Patent 57-78964*, 1983.

[2] H. Kajioka, H. Matsumura, "Single polarization optical fiber and its applications," *Hitachi Rev.*, vol. 33, pp. 215-218, 1984.

[3] C. Doerr, "Toward a noise-free interferometric fiber optic gyroscope," MIT-EE, Phd Thesis, 1994.

[4] C. Doerr, K. Tamura, M. Shirasaki, H. Haus, E. Ippen, "Orthogonal Polarization gyroscope with increased stability and resolution," *Applied Optics*, vol. 33, no. 34, pp. 8062-8068, 1994.

[5] Newport, "Optics Catalog," 1997-98.

[6] R. Berg, H. Lefevre, H. Shaw, "Compensation of the optical Kerr effect in fiber-optic gyroscopes," *Optics Letters*, vol. 7, pp. 282-284, 1982.

[7] R. Berg, B. Culshaw, C. Cutler, H. Lefevre, H. Shaw, "Source statistics and the Kerr effect in fiber-optic gyroscopes," *Optics Letters*, vol. 7, pp. 563-565, 1982.

[8] S. Alexander, "Design of wide-band optical heterodyne balanced mixed recievers," *J. Lightwave Technology*, vol. 5, pp. 523-537, 1987.

[9] K. Takada, "Calculation of Rayleigh backscattering noise in fiber-optic gyrosopes," *J. Optical Society of America*, vol. A2, pp. 872-877, 1985.

[10] E. Kintner, "Polarization control in optical-fiber gyroscopes," *Optics Letters*, vol. 6, pp. 154-156, 1981.

[11] Hotate, Tabe, "Drift of an optical fiber gyroscope by the Faraday effect: influences of the Earth's magnetic field," *Applied Optics*, vol. 25, no. 7, pp. 1086-1092, 1986.

[12] Hotate, Tabe, "Drift of an optical fiber gyroscope caused by the Faraday effect: experiment," *Applied Optics*, vol. LT-5, no. 7, pp. 997-1001, 1987.

[13] H. Lefevre, "The Fiber-Optic Gyroscope," Artech House, London, 1992.

[14] C. Lofts, P. Ruffin, J. Sawyer, "Development of sensing coils for an ultraminiaturized tactical fiber gyroscope," *SPIE Fiber Optic and Laser Sensors XI*, vol. 2070, pp. 142-151, 1993.

Appendix A: Mathcad Analysis

This Appendix contains the code to the Mathcad file that contains the analysis for the OPFOG. Each section contains the references that were used in that section of the analysis.

Define fundamental units:

$m := 1$ $cm := .01 \cdot m$ $mm := 10^{-3} \cdot m$

$\mu m := 10^{-6} \cdot m$ $nm := 10^{-9} \cdot m$ $km := 10^{3} \cdot m$

$in := 2.54 \cdot cm$

$sec := 1$ $ps := 10^{-12} \cdot sec$ $min := 60 \cdot sec$

$hr := 3600 \cdot sec$

$Hz := \dfrac{1}{sec}$ $MHz := 10^{6} \cdot Hz$

$W := 1$ $mW := 10^{-3} \cdot W$ $\mu W := 10^{-6} \cdot W$

$C := 1$ $F := 1$ $H := 1$

$J := W \cdot sec$ $A := \dfrac{C}{sec}$

$rad := 1$ $\mu rad := 10^{-6} \cdot rad$ $turn := 2 \cdot \pi \cdot rad$

$deg := \dfrac{\pi}{180} \cdot rad$ $arcsec := \dfrac{deg}{3600}$ $arcmin := \dfrac{deg}{60}$

$V := \dfrac{W}{C}$ $mV := 10^{-3} \cdot V$

$\Omega := 1$ $M\Omega := 10^{6} \cdot \Omega$

$Gauss := 1$ $Oe := 1 \cdot Gauss$

$degC := 1$ $ppm := 10^{-6}$ $dB := 1$

Define Constants:

$h := 1.054 \cdot 10^{-34} \cdot J \cdot sec$ The Plank's (this is "h bar") const;

$e := 1.6021892 \cdot 10^{-19} \cdot C$ The electron charge in Coulombs

$c := 299702590 \cdot \dfrac{m}{sec}$ The speed of light

$\varepsilon o := 8.8542 \cdot 10^{-12} \cdot \dfrac{F}{m}$ Permittivity of free space

$\mu o := 4 \cdot \pi \cdot 10^{-7} \cdot \dfrac{H}{m}$ Permeability of free space

$kb := 1.3807 \cdot 10^{-23}$ Boltzmann's constant in J/degK

$Earth\_Rate := 10.4 \cdot \dfrac{deg}{hr}$ Earth rate at Boston

$E := 2.71828$ ln(E)=1

Define Gyro Constants:

Source:

$\lambda := 1550 \cdot nm$ Center wavelength of Anritsu SLD

$\Delta\lambda := 64.8 \cdot nm$ The optical source linewidth

$\nu := \dfrac{c}{\lambda}$ Optical frequency

$Pin := 1 \cdot mW$ The input power from source

$d\lambda\_dT := 300 \cdot ppm$ The wavelength sensitivity to temperature

$dI\_dT := 100 \cdot ppm$ The wavelength sensitivity to current

Fiber:

$ncore := 1.457$ The index of refraction of the fiber core - pure silica core

$nclad := (1 - .035 \ \%) \cdot ncore$ The index of refraction of the fiber cladding

$nclad = 1.45649$

$\Delta n := ncore - nclad$ The difference in fiber index

$\Delta n = 5.0995 \cdot 10^{-4}$

$Hparam := 1.5 \cdot 10^{-4} \cdot \dfrac{1}{m}$ H-parameter of fiber

$Lbeat := \dfrac{\lambda}{\Delta n}$ Beatlength of fiber

$Lbeat = 3.03951 \cdot 10^{-3}$

$frozentwist := 0.004 \cdot \dfrac{rad}{m}$ Fiber twist frozen into fiber from manufacturer - estimate

$Dmode := 10.5 \cdot \mu m$ The mode field diameter

$Dcore := 9.0 \cdot \mu m$ The fiber core diameter

$Dclad := 125 \cdot \mu m$ The fiber cladding diameter

$Djac := 160 \cdot \mu m$ Fiber jacket outside diameter

Fiber (cont)

$dn\_dT \quad := \quad 1.35 \cdot 10^{-5} \cdot \dfrac{1}{degC}$

Index change with temperature

$\alpha lin \quad := \quad 5.5 \cdot 10^{-7} \cdot \dfrac{1}{degC}$

Linear thermal expansion coefficient of fiber

$Loss\_Fiber \quad := \quad -1.6 \cdot \dfrac{dB}{km}$

Fiber insertion loss

$dL\_dT \quad := \quad 4 \cdot ppm$

Fiber length change with temperature

Coil:

$D \quad := \quad 6.8 \cdot in$

The coil diameter

$D = 0.17272 \qquad m$

$L \quad := \quad 1000 \cdot m$

The length of fiber used on coil

$N \quad := \quad \dfrac{L}{\pi \cdot D}$

The number of turns of fiber on c

$CoilExt \quad := \quad -36.6 \cdot dB$

The extinction ratio of the PM fiber coil - measured

$twist \quad := \quad \dfrac{1 \cdot turn}{1 \cdot m}$

Fiber twist parameter before unwinding machine - estimate

$TwistReduc \quad := \quad 100$

Reduction factor of 100 from unwinding machine - estimate

$LossCoil \quad := \quad Loss\_Fiber \quad \cdot L$

Coil insertion loss

$dD\_dT \quad := \quad 4 \cdot ppm$

Change in coil diameter with temperature (combination of fibe epoxy, and fiber support structur

Detector:

$\rho \quad := \quad 0.95 \cdot \dfrac{A}{W}$

Responsivity of Epitaxx detector

$\eta \quad := \quad 1 \ - \ \dfrac{h \cdot c \cdot \rho}{e \cdot \lambda}$

Quantum efficiency of detector

$Bd \quad := \quad 2.6 \cdot MHz$

Detection bandwidth of gyro

$Rtrans \quad := \quad 10 \cdot M\Omega$

Transimpedance resistance of detector

61

Si Prism:

nPrism := 3.49   Index of refraction of Si

nair := 1   Index of refraction of air

ϵpr := 0.1 · deg   Error in aligning beam
                                   perpendicular to prism face

$$\Theta B := atan \left(\frac{nair}{nPrism} \right)$$ Brewster angle of prism

$$\Theta B \cdot \frac{360}{2 \cdot \pi} = 15.98875 \qquad deg$$

$$\Theta out := asin \left(\frac{nPrism}{nair} \cdot sin (\Theta B) \right)$$ The ideal output angle of the
                                                                                   Si prism

$$\Theta out \cdot \frac{360}{2 \cdot \pi} = 74.01125 \qquad deg$$

$$\Theta err := asin \left(\frac{nair}{nPrism} \cdot sin (\epsilon pr) \right)$$ The error angle within Si
                                                                                      prism

$$\Theta max := asin \left(\frac{nPrism}{nair} \cdot sin (\Theta B + \Theta err) \right)$$ The maximum output
                                                                                                angle of the Si prism

$$\Theta max \cdot \frac{360}{2 \cdot \pi} = 74.36401 \qquad deg$$

$$\Theta min := asin \left(\frac{nPrism}{nair} \cdot sin (\Theta B - \Theta err) \right)$$ The minimum output
                                                                                                angle of the Si prism

$$\Theta min \cdot \frac{360}{2 \cdot \pi} = 73.66585 \qquad deg$$

$$(\Theta max - \Theta min) \cdot \frac{360}{2 \cdot \pi} = 0.69816$$ The angular error from input
                                                                          alignment

tTM := 95 %   The power transmission
                                   coeffient of TM polarization

tTE := 43.7 %   The power transmission
                                   coeffient of TE polarization

rTE := 29.4 %   The power reflection
                                   coeffient of TE polarization

ETEK Beamsplitter:

BSExt := − 28 · dB

The extinction ratio of the beamsplitter before the coi conservative estimate

k := 0.491

The splitting ratio of the BC into the coil - measured

Temperature:

Op_Temp := 50 · degC

Operating temperature of system

ΔT := 0.1 · degC

Temperature control of gvrc

$\Delta Tgrad$:= 0.001 · $\frac{degC}{hr}$

Temperature gradient between inner and outer fiber layer per hour

Optical Fiber Splice:

Splice_ext := − 40 · dB

Polarization alignment of a PM fiber

Loss_Splice := − 0.1 · dB

Splice insertion loss

Miscellaneous:

α := 6.47 · 10^{-4} · $\frac{rad}{degC}$

Temperature coefficient of $\lambda/4$ Plate - measured

MagShield := 100

Magnetic shielding factor 100 with shielding

RIN_Flag := 1

Flag for RIN control - dependant upon approach
0 - differencing
1- sum/difference

B := 1 · Hz

Detection bandwidth of gvrc

Recirculator:

Isolation := 39 · dB

Return loss from output bac to input

Errors:

$$QWP\_temp\_err \quad := \quad \alpha \cdot \Delta T$$

λ/4 plateretardation error due to temperature

$$pbr \quad := \quad 26.9 \quad \%$$

Power backreflection from Si prism

$$pTM\_err \quad := \quad 5 \quad \%$$

Power reflection error in Si prism's Brewster angle

Component Insertion Loss Parameters:

$$LossRecirc \quad := \quad -0.8 \cdot dB$$

The insertion loss of the JDS recirculator

$$LossPol \quad := \quad -0.71 \cdot dB$$

The insertion loss of the input polarizer - measured

$$LossPrism \quad := \quad 10 \cdot log \ (\ pbr \ )$$

The loss of the Si Prism from backreflections

$$LossPrism \quad = \quad -5.7 \quad dB$$

$$LossTE \quad := \quad 10 \cdot log \ (\ tTE \ )$$

The loss of the Si Prism from transmitting some of the TE field

$$LossTE \quad = \quad -3.6 \quad dB$$

$$LossETEK \quad := \quad -0.56 \cdot dB$$

The insertion loss of the ETEK beamsplitter - measured

$$Loss\_to\_coil \quad := \quad LossPol \quad + \quad LossRecirc \quad + \quad LossTE \quad + \quad LossPrism$$

The losses up to input of coil

$$Po \quad := \quad Pin \cdot 10^{\frac{Loss\_to\_coil}{10}}$$

Power launched into coil BS

$$LossTotal \quad := \quad 2 \cdot LossPrism \quad + \quad LossTE \quad + \quad 2 \cdot LossETEK \quad + \quad LossCoil$$

The insertion loss of the system in dB

$$LossTotal \quad = \quad -17.72 \quad dB$$

Calculation of Power on the Detector:

$$Pdet := Pin \cdot \left[10^{\left(\frac{LossTotal}{10} \right)} \right]$$

The optical power falling on the detector (AC and DC)

$$Pdet = 1.69039 \cdot 10^{-5} \ W$$

The Calculation of the Gyro Scale Factor:

$$K := \frac{\lambda \cdot c}{2 \cdot \pi \cdot D \cdot L}$$

Open loop scale factor

$$K = 0.42806 \quad \text{rad/sec / rad}$$

The Calculation of the Shot Noise:

$$Shot\_Noise := 2 \cdot \sqrt{\frac{h \cdot \nu}{\eta \cdot Pdet}}$$

NOTE: The normal shot noise equation is doubled because the detection scheme requires two detectors

$$Shot\_Noise = 7.40632 \cdot 10^{-8} \quad \text{rad/rt-Hz}$$

The Calculation of the RIN Noise:

$$RIN := \sqrt{\frac{\lambda^2}{2 \cdot c \cdot \Delta\lambda}}$$

Relative Intensity Noise of the source

$$RIN = 2.48705 \cdot 10^{-7} \quad \text{rad/rt-Hz}$$

$$RIN := RIN \cdot RIN\_Flag$$

RIN after reduction

$$RIN = 2.48705 \cdot 10^{-7} \quad \text{rad/rt-Hz}$$

The Calculation of the Johnson Noise:

$$Njohn := \sqrt{\frac{4 \cdot kb \cdot (Op\_Temp + 273)}{Rtrans \cdot \rho^2 \cdot Pdet^2}}$$

Thermal noise from detector

$$Njohn = 2.63009 \cdot 10^{-9} \quad \text{rad/rt-Hz}$$

The Calculation of the Thermal Noise:

Knudsen, et. al. "Measurements of Fundamental Thermal Induced Phase Fluctuations in the Fiber of a Sagnac Interferometer"
IEEE Photonics Technology Letters, Vol 7, pg 90-92, 1995.

$\text{Temp} := 273 + \text{Op\_Temp}$ Operating temperature in degK

$\kappa := 1.37 \cdot \dfrac{W}{m \cdot degC}$ Thermal conductivity

$td := 0.82 \cdot 10^{-6} \cdot \dfrac{m^2}{sec}$ Thermal diffusity

$v := \dfrac{c}{ncore}$ Velocity of light in fiber

$kmax := \dfrac{4}{Dmode}$

$kmin := \dfrac{4.81}{Dclad}$

$\omega := 2 \cdot \pi \cdot 100 \cdot Hz$ Frequency of operation

$c1 := kmax^2 + \left(\dfrac{\omega}{v}\right)^2$ $c2 := kmin^2 + \left(\dfrac{\omega}{v}\right)^2$

$c3 := \dfrac{\omega}{td}$

$\text{varience} := \sqrt{\dfrac{\pi \cdot kb \cdot L}{\kappa} \cdot \ln\left[\dfrac{(c1)^2 + (c3)^2}{(c2)^2 + (c3)^2}\right] \cdot \left[1 - \dfrac{\sin\left(\dfrac{\omega \cdot L}{v}\right)}{\left(\dfrac{\omega \cdot L}{v}\right)}\right]}$

$\text{Therm\_Noise} := \dfrac{2 \cdot \text{Temp}}{\lambda} \cdot (dn\_dT + ncore \cdot \alpha lin) \cdot \text{varience}$

Noise due to thermal fluctuations

$\text{Therm\_Noise} = 3.95286 \cdot 10^{-9}$ rad/rt-Hz

The Minimum Detectable Rotation Rate:

$$\text{Noise} := \sqrt{\text{Shot\_Noise}^2 + \text{RIN}^2 + \text{Njohn}^2 + \text{Therm\_Noise}^2}$$

Total noise of the system

$$\phi\text{min} := \frac{\text{Noise}}{\cos\left[\dfrac{(\text{QWP\_temp\_err})}{2}\right]}$$

NOTE: The cosine term is due to biasing errors from the $\lambda/4$ plate

$$\phi\text{min} = 2.59542 \cdot 10^{-7} \quad \text{rad/rt-Hz}$$

$$\Omega\text{min} := \phi\text{min} \cdot \text{K} \cdot \frac{360}{2 \cdot \pi} \cdot 3600$$

$$\Omega\text{min} = 0.02292 \qquad \text{deg/hr / rt-Hz}$$

$$\text{Psd } \Omega\text{min} := \Omega\text{min}^2 \cdot \frac{1}{\sqrt{2}}$$

$$\text{Psd } \Omega\text{min} = 3.71321 \cdot 10^{-4} \qquad \text{RMS (deg/hr}^2 \text{/Hz}$$

$$\text{Psd } \Omega\text{min} := \sqrt{\text{Psd } \Omega\text{min} \cdot \frac{B}{\text{hr}}}$$

$$\text{Psd } \Omega\text{min} = 3.21161 \cdot 10^{-4} \qquad \text{deg/rt-hr}$$

The Calculation of Polarization Bias Error

ConLdB   := − 30.0 · dB

The polarization crosstalk on launch 1 a coil is defined by IaB/aAI. If using active alignment, this value could be as low as -35dB. Hand alignment yields -25dB.

CinFdB   := CoilExt   + BSExt

The crosstalk in the fiber defined by ItAB/tAAI. The extra factor is from th₁ PBS. The PBS strips the polarization into which most of the error is accumulated in the second pass of li through the fiber from crosscoupling i fast axis of the coil.

pedB   := 2 · BSExt

The effective extinction through the PBS. It is doubled bacause the be an traverses it twice.

$$PolExt := \sqrt{10^{\frac{pedB}{10}}}$$

The polarizer extinction in amplitude form.

$$ConL := \sqrt{10^{\frac{ConLdB}{10}}}$$

The launch crosstalk in amplitude form.

$$CinF := \sqrt{10^{\frac{CinFdB}{10}}}$$

The crosstalk in fiber in amplitude form.

$\phi_{\varepsilon}max$:= PolExt   · 2.0 · ConL · CinF

The maximum gyro error due to polarization.

$$\phi_{\varepsilon}max = 5.90242 \cdot 10^{-8} \quad rad$$

$$\Omega pol := \phi_{\varepsilon}max \cdot K \cdot 3600 \cdot \frac{360}{2 \cdot \pi}$$

The gyro bias drift due to polarization error.

$$\Omega pol = 5.21141 \cdot 10^{-3} \quad deg/hr$$

NOTE: For best realistic performance for bias drift, you should use active alignment for -35dB launch crosstalk. You need beamsplitters with -30dB polarization extinction. You need a coil that has at least -25dB extinction.

The Calculation of Polarization Bias Error - another way

Lefevre, "The Fiber-optic Gyroscope"
Artech House, pg 73-80, 1992.

$$Lc := \frac{\lambda^2}{\Delta\lambda}$$

Coherence length of source
$$Lc = 3.70756 \cdot 10^{-5} \quad m$$

$$Ld := Lc \cdot \frac{Lbeat}{\lambda}$$

Depolarization length
$$Ld = 0.0727 \quad m$$

$$Ncoup := \frac{L}{Ld}$$

Number of coupling points in fiber
$$Ncoup = 1.38 \cdot 10^4$$

$$Cons := 10^{\frac{CoilExt}{10}}$$

Extinction of coil

$$\varepsilon BS := \sqrt{10^{\frac{BSExt}{10}}}$$

Beamsplitter extinction in amplitude form
$$\varepsilon BS = 0.03981$$

$$\sigma coup := \varepsilon BS^2 \cdot \frac{Cons}{\sqrt{Ncoup}}$$

RMS phase deviation
$$\sigma coup = 2.95652 \cdot 10^{-9} \quad rad$$

$$\Omega coup := K \cdot \sigma coup \cdot 3600 \cdot \frac{360}{2 \cdot \pi}$$

Bias due to polarization coupling
$$\Omega coup = 2.61039 \cdot 10^{-4} \quad deg/h$$

The Calculation of Bias from Kerr Effect

Frigo, et. al. "Optical Kerr effect in fiber gyroscopes: effects of non-chromatic sources" Optics Letters, Vol 8, pg 119-121, 1983.

$$\Delta\beta := \frac{2 \cdot \pi \cdot \Delta n}{\lambda}$$

The difference in propagation constants

$$\Delta\beta = 2.06717 \cdot 10^{3} \text{ rad/m}$$

$$\beta kerr := 7.4 \cdot 10^{-19} \cdot \frac{m}{\mu W}$$

The Kerr coefficient

$$Amode := \pi \cdot \left(\frac{Dmode}{2}\right)^{2}$$

The mode field area

$$Amode = 8.65901 \cdot 10^{-11} \text{ m}^2$$

$$Po := Pin \cdot 10^{\frac{Loss\_to\_coil}{10}}$$

Power launched into coil BS

$$\Gamma := (2.097 \quad \%)^{2}$$

Coherence peak2-1% 1σ amplitude modulation measured

$$\xi := \frac{0.5 \cdot \beta kerr \cdot (1 - 2 \cdot k) \cdot Po}{Amode}$$

Kerr constant

$$\xi = 6.38616 \cdot 10^{-9} \text{ m}^{-1}$$

$$Leff := \frac{\left(1 - E^{LossCoil}\right) \cdot km}{-LossCoil}$$

Effective fiber length [1]

$$Leff = 498.81454 \quad m$$

$$KerrBias := K \cdot \xi \cdot Leff \cdot \Gamma \cdot \frac{360}{2.0 \cdot \pi} \cdot 3600$$

Bias from Kerr Effect

$$KerrBias = 1.2368 \cdot 10^{-4} \text{ deg/hr}$$

The Calculation of Kerr Effect Bias - Another Way

Bergh, et. al. "Compensation of the optical Kerr effect in fiber-optic gyroscopes" Optics Letters, Vol 7, pg 282-284, 1982.

Bergh, et. al. "Source statistics and the Kerr effect in fiber-optic gyroscopes" Optics Letters, Vol 7, pg 563-565, 1982.

$$\eta n2 \ \delta \ := \ 10^{-14} \cdot \frac{\mu m^2}{\mu W}$$

Approximate Kerr coefficient of the silic fiber [1]

$$Acore \ := \ \pi \cdot \left(\frac{Dcore}{2} \right)^2$$

Cross-sectional area of fiber core

$$Po \ := \ Pin \cdot 10^{\frac{Loss\_to\_coil}{10}}$$

Power launched into coil BS

$$Po \ = \ 8.30297 \cdot 10^{-5} \quad W$$

$$Nmodes \ := \ 10^4$$

Approximate number of modes in SLD source

$$\Omega kerr \ := \ \frac{2 \cdot c \cdot \eta n2 \ \delta}{D \cdot Acore} \cdot (1 - 2 \cdot k) \cdot \frac{Po}{Nmodes} \cdot 3600 \cdot \frac{360}{2 \cdot \pi}$$

Bias from Kerr Effect
Nmodes from [2]

$$\Omega kerr \ = \ 1.68164 \cdot 10^{-5} \quad deg/h\iota$$

The Calculation of Faraday Effect Bias

Hotate and Tabe, "Drift of an optical fiber gyroscope by the Faraday effect: influn of the Earth's magnetic field", Applied Optics, Vol 25, No 7, pg 1086-1092, 1986.

Hotate and Tabe, "Drift of an Optical Fiber Gyroscope Caused by the Faraday Effect: Experiment", Journal of Lightwave Technology, Vol LT-5, No 7, pg 997-1001, 1987.

CRC Handbook of Chemistry and Physics, pg 12.164,1997.

Note: Conversion between Gau(ss) and Oersted(Oe)
Maxwell's Eqns: $B = \mu_0 H$

$\mu_0 = 4\pi \ 10^{-7} \ H/m = 4\pi \ 10^{-7} \ Wb/(A \ m)$
$1 \ Oe = 10^3/(4\pi) \ A/m$

$\mu_0 \cdot H = (4\pi \ 10^{-7} \ Wb/Am) * (1000/4\pi \ A/m)$
$\qquad = 10^{-4} \ Wb/m^2$
$\qquad = 1 \ Gauss$

$$Vfe := 0.013 \ \cdot \ \frac{arcmin}{Oe \cdot cm}$$

Verdet constant of fiber [3]

$$Vfe = 3.78155 \ \cdot 10^{-4} \ rad/(Gauss \ m)$$

$$twist := \frac{twist}{TwistReduc}$$

Fiber twist in system

$$Wfe := \left(\frac{twist}{2 \cdot \sqrt{2}}\right)^2 \cdot \frac{rad^2}{m^2}$$

Spectral twist characteristic of fiber

$$Bmag := 1 \cdot Gauss$$

Magnetic field amplitude

$$\zeta := Vfe \ \cdot \ \frac{Bmag}{MagShield}$$

Faraday Rotation per unit length

$$\zeta = 3.78155 \ \cdot 10^{-6} \qquad rad/m$$

$$\Delta\phi := \frac{4 \cdot \zeta \cdot D}{\Delta\beta} \cdot \sqrt{2 \cdot \pi \cdot N \cdot Wfe}$$

Phase difference due to magnetic field [1,

$$\Delta\phi = 3.02117 \ \cdot 10^{-9} \qquad rad$$

$$\Omega farad := \Delta\phi \cdot K \cdot 3600 \ \cdot \frac{360}{2 \cdot \pi}$$

Bias due to Faraday Effect

$$\Omega farad = 2.66747 \ \cdot 10^{-4} \qquad deg/h$$

The Calculation of Rayleigh Backscattering Bias

Takada, "Calculation of Rayleigh backscattering noise in fiber-optic gyroscopes" Optical Society of America, Vol A2, pg 872-877, 1985.

Brinkmeyer, "Backscattering in single-mode fibres," Electronic letters, Vol16, pg 329-330, 1980.

Bohm, et.al., "Low-noise fiber-optic rotation sensing," Optics Letters, Vol 6, No 2, 64-66, 1981.

Derickson, "Fiber Optic Test and Measurement," Prentice Hall, pg 448, 1998.

Saleh, Teich, "Fundamentals of Photonics," John Wiley & Sons, pg 279-280, 199

$$\alpha r := \frac{0.76 + 0.51 \cdot \Delta n}{\left(\lambda \cdot 10^{6}\right)^{4}}$$

Rayleigh scattering loss in dB/km for Germanium doped fiber [4]

$$\alpha r := E^{\frac{-\alpha r}{10}} \cdot \frac{1}{km}$$

Rayleigh scattering coefficient

$$Lc := \frac{\lambda^{2}}{\Delta \lambda}$$

Coherence length of source

$$Lc = 3.70756 \cdot 10^{-5} \, m$$

$$Tr := 0.01 \cdot sec$$

Coherence time of Rayleigh scattered due to environmental fluctuations- Not NOT coherence time of source [3]

$$NA := \sqrt{ncore^{2} - nclad^{2}}$$

Numerical aperture of fiber

$$NA = 0.03855$$

$$Vf := 2 \cdot \pi \cdot \frac{Dcore}{2 \cdot \lambda} \cdot NA$$

V parameter of the fiber [5]

$$Vf = 0.70312$$

$$\omega := 0.65 + 1.619 \cdot Vf^{-1.5} + 2.879 \cdot Vf^{-6}$$

Normalised spot-size ω_0/a [2]

$$S := \frac{1.5}{\omega^{2} \cdot V^{2}} \cdot \frac{ncore^{2} - nclad^{2}}{ncore^{2}}$$

Backscattering factor [2]

$$S = 1.41667 \cdot 10^{-6}$$

$$\Omega ray := K \cdot (1 - 2 \cdot k) \cdot \sqrt{\frac{Lc \cdot S \cdot \alpha r \cdot Tr \cdot B}{2 \cdot ncore}} \cdot 3600 \cdot \frac{360}{2 \cdot \pi}$$

Bias from Rayleigh Scattering [1]

$$\Omega ray = 2.11968 \cdot 10^{-5} \quad \text{deg/hr}$$

The Calculation of Thermal Non-Reciprocity Bias

Shupe, "Thermally induced nonreciprocity in the fiber-optic interferometer" Applied Optics, Vol 19, No 5, pg 654-655, 1980.

$$\Omega therm := \Delta Tgrad \cdot \frac{ncore \cdot L^2}{6 \cdot N \cdot \pi \cdot D^2} \cdot (dn\_dT + ncore \cdot \alpha lin)$$

$$\Omega th := \Omega therm \cdot 3600 \cdot \frac{360}{2 \cdot \pi}$$

Bias from thermal gradients in the fiber

$$\Omega th = 1.15203 \cdot 10^{-3} \quad \text{deg/hr}$$

Total Bias

$$TBias := \sqrt{\Omega pol^2 + \Omega kerr^2 + \Omega ray^2 + \Omega th^2 + \Omega farad^2}$$

$$TBias = 5.34395 \cdot 10^{-3} \quad \text{deg/hr}$$

$$TotalBias\_Error := TBias \cdot \frac{1}{6} \quad 1\sigma \text{ bias}$$

$$TotalBias\_Error = 8.90658 \cdot 10^{-4} \quad \text{deg/hr}$$

The Calculation of Scale Factor Errors

$$dK\_dD \; := \; \frac{2 \cdot \pi \cdot L}{\lambda \cdot c}$$

Scale Factor change due to diameter term

$$dK\_dD \; \cdot \; dD\_dT \; = \; 5.41025 \quad \cdot 10^{-5} \; \text{ppm}$$

$$dK\_dL \; := \; \frac{2 \cdot \pi \cdot D}{\lambda \cdot c}$$

Scale Factor change due to length term

$$dK\_dL \; \cdot \; dL\_dT \; = \; 9.34459 \quad \cdot 10^{-9} \; \text{ppm}$$

$$\lambda\, reduc \; := \; 100$$

Optical source wavelength control loop reduct factor

$$d\lambda\_dT \; := \; \frac{d\lambda\_dT}{\lambda\, reduc}$$

Reduction due to feedback loop control

$$dK\_d\,\lambda \; := \; \frac{2 \cdot \pi \cdot L \cdot D}{\lambda^2 \cdot c}$$

Scale Factor change due to wavelength term

$$dK\_d\,\lambda \cdot d\lambda\_dT \; = \; 4.52158 \quad \text{ppm}$$

$$SF1 \; := \; dK\_dD \; \cdot \; dD\_dT$$

$$SF2 \; := \; dK\_dL \; \cdot \; dL\_dT$$

$$SF3 \; := \; dK\_d\,\lambda \cdot d\lambda\_dT$$

$$SFstability \; := \; \sqrt{(\,SF1\,)^2 + (\,SF2\,)^2 + (\,SF3\,)^2}$$

Total scale factor change from temperature changes and source wavelength changes

$$SFstability \quad = \; 4.52158 \quad \text{ppm}$$

Bias due to Quarter Waveplate

$$qwp\_retard\_err \quad := \quad \alpha \cdot \Delta T$$

Retardation change from temperature in quarter waveplate

$$qSF1 \quad := \quad \sin \; (\; qwp\_retard\_err \quad) \cdot 10^{6}$$

Scale factor error from temperature variations across quarter waveplate

$$qSF1 \quad = \quad 64.7 \qquad ppm$$

$$\lambda\_control \quad := \quad 1 \cdot ppm$$

Control of source wavelength shift - assuming wavelength control/stabilization

$$source\_retard\_err \quad := \quad \frac{\pi}{2} \cdot \lambda\_control$$

Retardation change from source wavelength shift

$$qSF2 \quad := \quad \sin \; (\; source\_retard\_err \quad) \cdot 10$$

Scale factor error from wavelength shifts in source changing waveplate retardation

$$qSF2 \quad = \quad 1.5708 \qquad ppm$$

Coil Design Issues

Lofts, et.al., "Development of sensing coils for an untraminiaturized tactical fiber gyroscope," SPIE Fiber Optic Laer Sensors XI, Vol 2070, pg 142-151, 1993.

$$Rc \quad := \quad \frac{Dcore}{2 \cdot NA^{2}}$$

Critical bend radius where optical loss sharply increases

$$Rc \quad = \quad 3.02881 \quad \cdot 10^{-3} \qquad m$$